Observations and Numerical Simulations of the Origin and Development of Very Large Snowflakes

R. PAUL LAWSON

SPEC, Inc., Boulder, Colorado

RONALD E. STEWART

Climate Processes and Earth Observation Division, Atmospheric Environment Service, Downsview, Ontario, Canada

LEIGH J. ANGUS*

SPEC, Inc., Boulder, Colorado

(Manuscript received 18 December 1996, in final form 9 December 1997)

ABSTRACT

The Canadian Atlantic Storms Program (CASP II) field experiment was conducted near St. John's, Newfoundland, Canada, during January–March 1992, and it focused on the nature of winter storms. Analyses of CASP II aircraft, surface, satellite, and radar observations collected during an intensive study of the origin and development of 9 mm h^{-1} precipitation containing 4–5-cm diameter snowflakes are compared in this article with results of the MM5 (mesoscale) and Mitchell (microphysical) models. MM5 simulations of the thermal, kinematic, and bulk microphysical fields were in good agreement with the observations; this comparison provided the basis for extending the spatial and temporal scales of the aircraft observations to a larger-scale domain using the model results. The Mitchell analytical–numerical model was used to improve the understanding of the microphysical processes that led to the development of the very large snowflakes. A synthesis of results using the different techniques leads to the conclusion that the snowflakes originated as 3–5-mm dendritic crystals in an area of weak convective instability at 5 km and were transported downwind in a strongly sheared airflow. The dendrites aggregated, fell into an existing snowzone (supported in some regions by vertical motion with velocities ranging from 0.2–0.6 m s^{-1}), and continued to descend along a deep, downward sloping layer with temperatures near 0°C. Rapid aggregation occurred in the near 0°C region in particular and without appreciable particle breakup. An exponential fit to the particle size distribution in the region of very large snowflakes had a slope parameter on the order of 100 m^{-1}.

1. Introduction

Winter storms that result in the production of very large snowflakes and heavy snowfall in the vicinity of populated areas can have a significant social–economic impact. Such storms are typically associated with the rapid accumulation of snowfall at the surface (Auer 1971; Lawson et al. 1993a), making snow removal difficult and presenting a hazard to surface travel.

Surface observations of very large[1] snowflakes occurring within winter storms have been well-documented for over a century (e.g., Lowe 1887; Plunket 1891; Denning 1912; Abbe 1915; Hawke 1951; Auer 1971; Corliss 1984; Pike 1988; Stewart et al. 1990; Lawson et al. 1993a). However, there has been no observational and modeling study to date that has described the origin and development of outsized snowflakes, although it has been noted that both the rate of snowfall and size of the snowflakes typically peak when the temperature is near 0°C at the surface (see e.g., Magono 1953; Stewart 1992).

The second Canadian Atlantic Storms Program

*Current affiliation: National Oceanic and Atmospheric Administration, Boulder, Colorado.

Corresponding author address: Dr. R. Paul Lawson, SPEC, Inc., 5401 Western, Boulder, CO 80301.
E-mail: plawson@specinc.com

[1] Here we adopt the definition given by Lawson et al. (1993a) that "large" snowflakes are >2 cm and "very large" snowflakes are >4 cm in maximum dimension.

(CASP II) was conducted in January–March 1992 and focused on the severe maritime storms that lash the coast of Newfoundland (Stewart 1991; Stewart and Crawford 1995). CASP II provided an opportunity to make unique aircraft and surface observations of the origin and development of very large snowflakes occurring within these storms. In addition, radar and satellite observations were available. To extend the observational efforts, results from numerical models are needed. The modeling work reported here was conducted using the Mesoscale Model Version 5 (MM5) (Anthes and Warner 1978; Anthes 1990) in the four-dimensional data assimilation (4DDA) mode. This facilitated the incorporation of routine radiosonde and surface observations, as well as special radiosondes and aircraft dropsonde observations assimilated into the model. In this way, the model was used as a diagnostic instead of a predictive tool. Because mesoscale models are computationally limited in the complexity of the microphysics they can support, a separate microphysical model was spawned from the kinematic and thermodynamic fields generated by MM5. The microphysical model, designed to compute the diffusional, accretional, and aggregational contributions to particle growth, was adapted from Mitchell (1988, 1990, 1994, 1995).

In this paper we present a possible mechanism to explain the origin and development of the very large snowflakes observed on 14 February 1992 over the North Atlantic Ocean approximately 350 km southwest of St. John's, Newfoundland, Canada. This was the best documented storm with this form of precipitation, although very large snowflakes were not uncommon during CASP I (Stewart et al. 1987) and CASP II storms. Based on a synthesis of aircraft, radar, and satellite observations, coupled with the 4DDA modeling study, it was found that the very large snowflakes observed near the surface originated upwind in a region of weak convective instability at an elevation of about 5 km. At this elevation, where the temperature was -17°C, dendritic crystals 3–5 mm in size were transported downwind due to a large vertical shear in the horizontal wind. The origin crystals subsequently fell through a region where low-level convergence and commensurate vertical atmospheric motion slowed their descent. There was rapid particle growth, primarily due to aggregation in this region, where the temperature was near 0°C. Aircraft measurements using a new imaging probe with a 125-cm^2 viewing area revealed ice water contents up to $\sim$1.8 g m^{-3} in the region containing the very large snowflakes. The spatial extent of the region agreed well with the duration of the event recorded later at the surface near St. John's, as did the equivalent rain rate of 9 mm h^{-1}.

In section 2, we discuss the instrumentation available for this research. Section 3 presents an overview of the in situ observations and lays the foundation for the subsequent synthesis of aircraft, radar, and satellite observations and model output discussed in section 4. In section 5 we summarize and interpret the results.

2. Instrumentation

Aircraft measurements were made using a Convair-580 research aircraft operated by the National Research Council (NRC) of Canada. The Convair-580 was equipped with standard sensors for measuring state parameters and air motion. It was extensively instrumented for microphysical measurements. A full summary of the calibrations, errors, and limitations of the instrumentation is detailed in Cober et al. (1995). Here we give only a brief description of the instruments used in this study. Cloud liquid water content (LWC) was measured using two King LWC probes (King et al. 1978), a forward scattering spectrometer probe (FSSP), and a Rosemount icing rod (Baumgardner and Rodi 1989). Particles were counted and sized using Particle Measuring Systems (PMS) FSSP, 2D-C (cloud), 2D-P (precipitation), and 2D-G (greyscale) probes described by Knollenberg (1970, 1981). The aircraft was also equipped with a new precipitation imaging probe that has about 30 times the sample volume and 7 times the viewing area of the PMS 2D-P probe. This probe, called a high-volume precipitation spectrometer (HVPS) and manufactured by SPEC Incorporated, was flown for the first time in CASP II and is described in Lawson et al. (1993a,b). The airborne ice water content (IWC) measurements presented here are based on analysis of images obtained with the HVPS. The Convair was also equipped with a Lightweight Loran Digital Dropsonde (L2D2) system made by the National Center for Atmospheric Research (NCAR). Photographs of instruments mounted under the wings of the Convair-580 and a close-up of the HVPS are shown in Fig. 1.

Surface, radar, and satellite observations were made in addition to the aircraft measurements. Ground-based temperature, wind, and precipitation measurements, along with photographs of the snowflakes, were taken by Atmospheric Environment Service (AES) personnel at Torbay, located 5 km north of the St. John's airport. A 5-cm wavelength weather radar with a range of 200 km was operated in scanning mode from a site at Holyrood, located 40 km southwest of the St. John's airport. Unfortunately, the digital recorder for this radar was inoperative on 14 February and only hard copies produced in real time are available for analysis. Additional radar measurements were recorded using the University of Toronto (UT) portable 3-cm Doppler radar (Thomson and List 1996) that was located at Torbay. The UT radar has a usable range of 30 km and was operated in both PPI and RHI modes. National Oceanic and Atmospheric Administration *GOES-7* and SSM/I satellite observations were also used in our analysis.

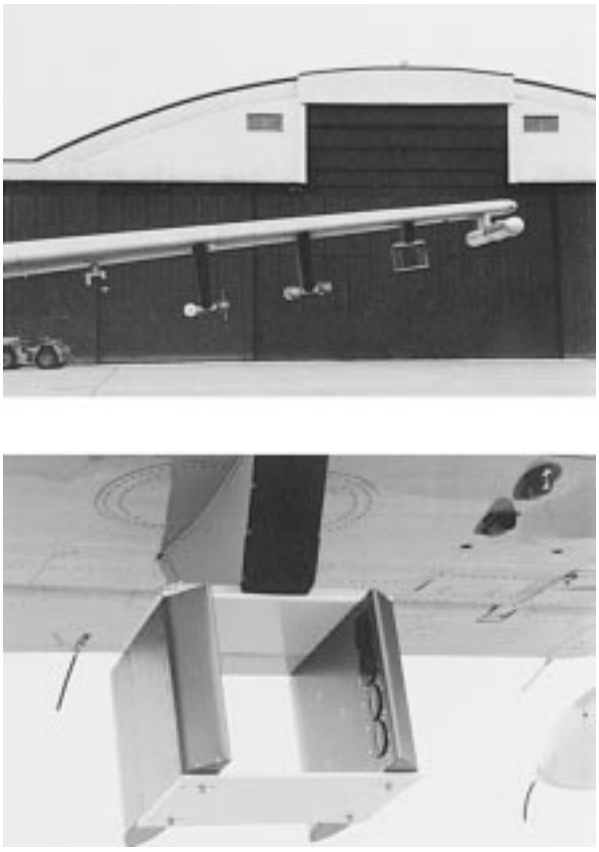

FIG. 1. Photographs showing (top) left wing of NRC Convair-580 research aircraft supporting (from left wing tip inward) electric field mill, HVPS, 2D-G, 2D-C, 2D-P, active scattering aerosol spectrometer probe, reverse-flow temperature, Rosemount temperature, and (bottom) close-up view of HVPS. The right wing (not shown) supported additional sensors, including another electric field mill, two FSSP probes, 1D-C, two King LWC probes, and a Rosemount icing rod.

3. Summary of in situ observations

A relatively weak center of low-pressure was analyzed at 0000 UTC on 14 February 1992 approximately 200 km east of Cape Hatteras, North Carolina, and tracked north along the east coast of the United States and then northeast off the east coast of Canada. The center of the low pressure was about 300 km south of the coast of Newfoundland by 0000 UTC 15 February. Aircraft observations were made from 1930 to 2330 UTC on 14 February. Figure 2 shows the position of the surface low at 0000 UTC 15 February and the aircraft track in both plan and profile views, incorporating thermodynamic, air motion, and microphysics measurements. Figures 2a,b,c are aligned so that the time and position information from one panel can be referenced by vertical registration to the other panels in the figure. For example, the wind and thermodynamic observations shown in Fig. 2b were analyzed from L2D2 dropsondes released during the first aircraft pass shown at 4.9 km in Fig. 2a, before the aircraft made the step-down traverses through the storm. The positions of the dropsonde releases are shown in the plan view in Fig. 2c.

The first aircraft leg began at 2003 UTC and was directed from northeast to southwest (shown going from right to left in Fig. 2a) at 4880-m (MSL) pressure altitude (545 mb). The air temperature at the northeast end of the leg was -20.5°C and increased monotonically (as shown in Fig. 2b) toward the warm front to -16.5°C at the southwest turnaround point. Until 2038 UTC, measurements of precipitation and cloud particles by the 2D-P and 2D-G probes showed mostly dendrites and unidentifiable habits <1 mm in size at concentrations of about 20 L^{-1}. Measurements from the PMS FSSP probe showed a flat distribution of particles in the 3–45 μm range with an average concentration of ~ 5 cm^{-3}. Heymsfield and Miloshevich (1989) have shown that FSSP concentrations of this magnitude in the presence of ice can be attributed to scattering from ice particles. This was supported in our measurements by an absence of supercooled LWC detected by the Rosemount icing rod.

At 2039 UTC, the aircraft encountered a region with strikingly different microphysical characteristics that extended for about 30 km at the southwest end of the first aircraft leg (Fig. 2). In this region, the temperature was -17°C, mean cloud droplet diameter was 21 μm, cloud droplet concentration was 25–40 cm^{-3}, and measurements by the FSSP and King probes showed LWC that ranged from 0.1 to 0.25 g m^{-3}. The mean diameter and LWC may be slightly overestimated by the FSSP because the measurements were in mixed-phase cloud, where scattering from ice particles may be interpreted as large drops by the FSSP. However, the average LWC measured by the FSSP in this region agreed to within about 10% of the King LWC measurement. These CASP II measurements compare to median in-cloud values of 0.1 g m^{-3} for LWC, 60–100 droplets cm^{-3}, and a median droplet diameter near 16 μm found by Isaac (1991) for all flights during CASP I conducted in 1986. Dendrites (including radiating assemblages) 3–5 mm in diameter were observed in concentrations of ~ 1 m^{-3}, and were often clumped together, as shown in Fig 3. Analysis of equivalent potential temperature (θ_e) from the dropsonde data shows that $d\theta_e/dz \leq 0$ in this region (Fig. 2), suggesting weak convective instability. Figure 2 also depicts this region of weak convective instability by the stippled area in the upper-left corner of the panel showing microphysical measurements.

Hobbs and Locatelli (1978) and Herzegh and Hobbs (1980) previously reported that midlevel instability was important for producing conditions necessary for the initial growth of small dendritic crystals that later grew through aggregation at lower altitudes. Regardless of the mechanism forming liquid cloud in this region, it is clear that circumstances were favorable for the initial rapid growth of dendrites; that is, the cloud was at water saturation and the water–ice saturation vapor pressure

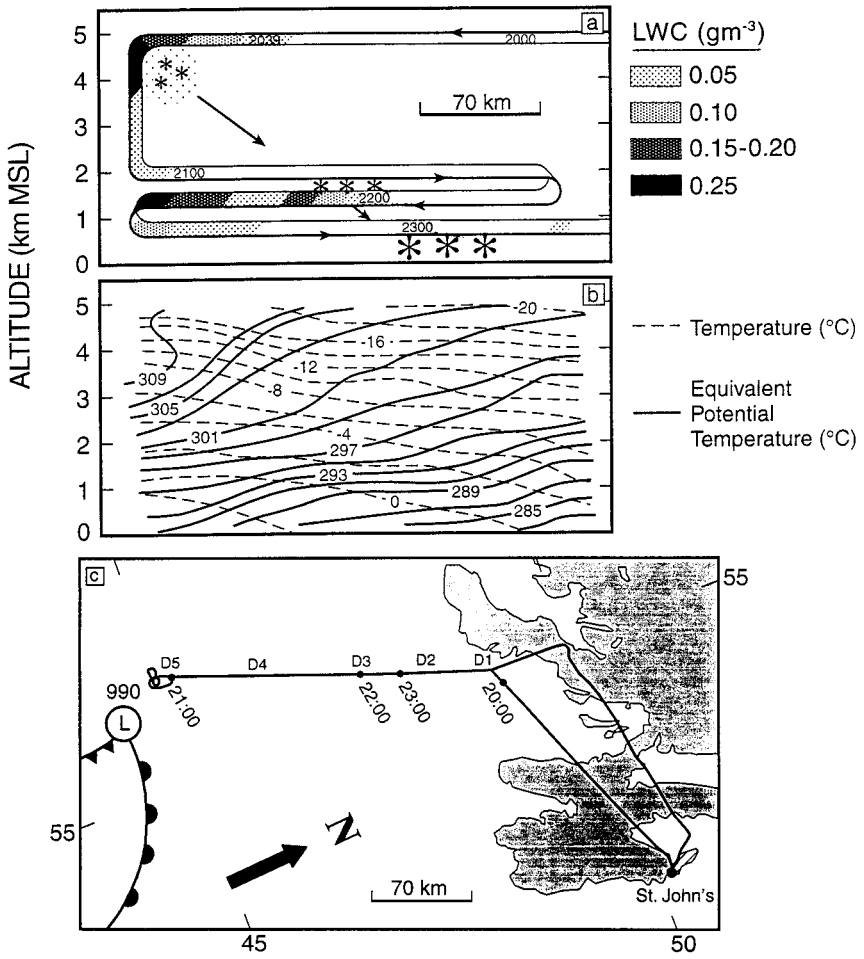

FIG. 2. (a) Profile view of flight track of Convair-580 research aircraft showing schematic depiction of measurements of LWC, region of weak convective instability (dotted region in upper left), and arrows depicting the trajectory of 2–5-mm dendrites at 4.9 km as they developed into 4–5-cm snowflakes at 0.6 km. Times in UTC are shown embedded within the flight track and correspond with the times shown in panel (c). (b) Profile view of temperature and equivalent potential temperature fields analyzed from five dropsondes released on the first pass shown in panel (a) at 4.9 km. (c) Plan view showing track of research aircraft from 1926–2330 UTC with the four aircraft passes stacked one on top of another. Surface fronts are from 2100 UTC analysis on 14 February 1992 and D1–D5 are positions of dropsondes released at 4.9 km.

difference reaches a maximum near −15°C. It is well known (e.g., Pruppacher and Klett 1978) that diffusional growth rates of ice crystals reach their maximum near −15°C due to vapor pressure differences and crystal shape considerations.

Information from three subsequent lower-level aircraft passes was examined in order to determine the evolution of the dendrites formed aloft (see Fig. 2). At 1830 m MSL (798 mb) the maximum observed snowflake diameter was 1 cm, at 1220 m (859 mb) it was 2–3 cm, and at 610 m (922 mb) it was 4–5 cm. The flight leg at 610 m (2230–2310) showed by far the most rapid evolution of particle size. The temperature decreased from about +6° to +0.5°C as the flight proceeded northeastward. Note that these (warmer) temperatures were measured 2 h later than the temperature field analyzed from dropsondes and shown in Fig. 2. For the first 25 min of this leg (~175 km), the 2D-G, 2D-P, and HVPS probes observed 1-mm raindrops and unmelted aggregates that did not exceed 1 cm in size. An example of images from the 2D-G and HVPS probes and typical particle spectra from the HVPS are shown in Fig. 4.

From 2259 to 2304 UTC, a dramatic shift in particle spectra was noted. The total concentration of particles decreased from about 0.5 m^{-3} to about 0.1 m^{-3} and aggregates of up to about 5 cm were observed over a 30-km region by the HVPS. Figure 5 shows images and histograms from two of the four HVPS channels. Very good agreement is seen between the two (identical)

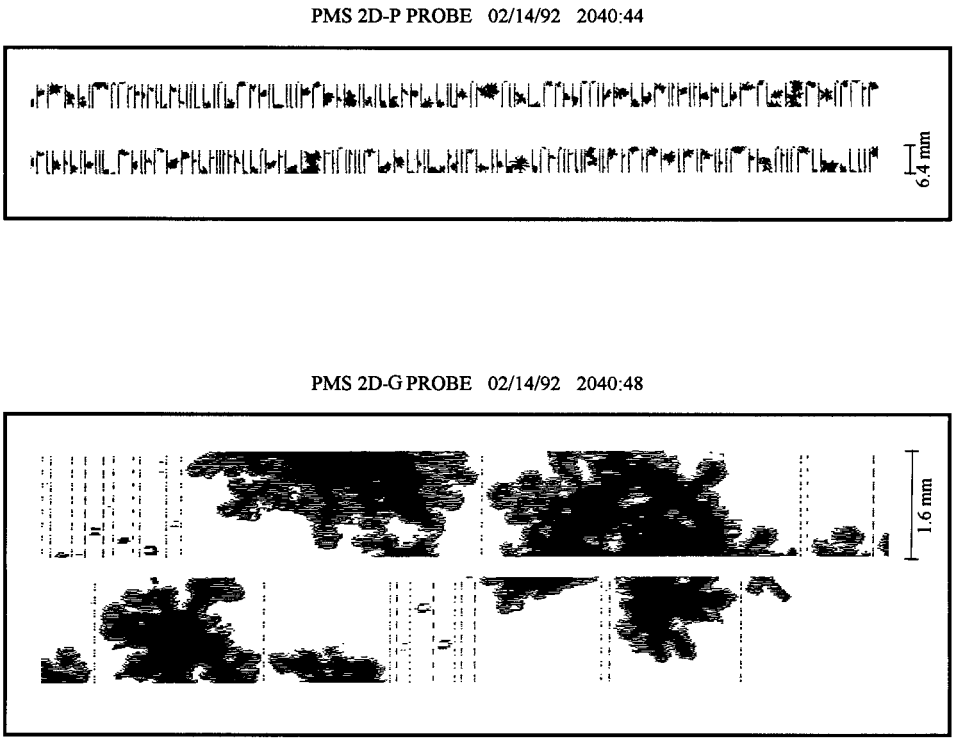

FIG. 3. Images from (top) 2D-P probe and (bottom) 2D-G probe of 2–5-mm dendritic ice particles observed in the region of convective instability shown in Fig. 2.

channels of the HVPS. This suggests that the relatively large sample volume of the HVPS ($\sim$1 m^3 s^{-1} per channel at the Convair average airspeed of $\sim$100 m s^{-1}) adequately samples the very large snowflakes over a spatial extent of 1 km.[2]

The region of very large snowflakes was also observed at the surface when it passed over the St. John's airport (Fig. 6). The period of rapid snowfall accumulation (peak rate up to 9 mm h^{-1}) coincides with arrival of the band identified by radar as the same region with very large snowflakes observed earlier by the Convair. The conditions shown in Fig. 6 are very similar to those often associated with observations of very large snowflakes; that is, the surface temperature is near 0°C and the wind is nearly calm (Stewart et al. 1990). In addition, the duration of the very large snowflake event (about 30 min) was used to estimate the spatial extent of the area containing the particles. Based on a band motion of 15–20 m s^{-1}, the width is on the order of 30 km.

Personnel on the ground collected snowflakes at Torbay during the period of rapid snowfall accumulation. The maximum dimensions of the snowflakes were observed to range in size from about 2 to 5 cm and there was evidence of only very light riming on some of the particles. Some of the snowflakes were also photographed and Fig. 7 shows one that is about 2 cm. This and other snowflakes were largely comprised of 1–5 mm dendritic crystals and needles, which are similar in appearance to the shadowgraphs shown in Fig. 3. Planar dendrites (e.g., types P1e and P1f), stellar dendrites (e.g., P1d), and radiating assemblages (P7b) typically form at water saturation in the temperature regime of $-13°$ to $-17°$C (Magono and Lee 1966), which corresponds with the altitude at which the initial 3–5-mm dendrites were observed with the aircraft. Rogers (1973) conducted a detailed observational study at the surface of 10 snowfalls in Laramie over a 13-month period. He photographed snowflakes, determined (when possible) their composition, and measured the unmelted and melted size distributions and snowfall rates. He noted that *all* aggregates larger than 1 cm were composed of planar dendrites or stellar dendrites, with needles present in small numbers. Rogers' observations are in good general agreement with Magono (1953), Jiusto (1971), Hobbs et al. (1971), and Rauber (1987). Stewart et al. (1990) also reported that most aggregates in CASP I storms were composed of dendrites and needles.

[2] This is the first time complete digital images of very large snowflakes have been recorded. In a previous CASP I study of Canadian winter storms near Nova Scotia (Stewart et al. 1990), surface observers measured very large snowflakes but the ground-based 2D-G digital imaging probe was limited to sizing snowflakes $<\sim$1 cm. This instrumentational limitation prompted the use of the new HVPS probe in CASP II.

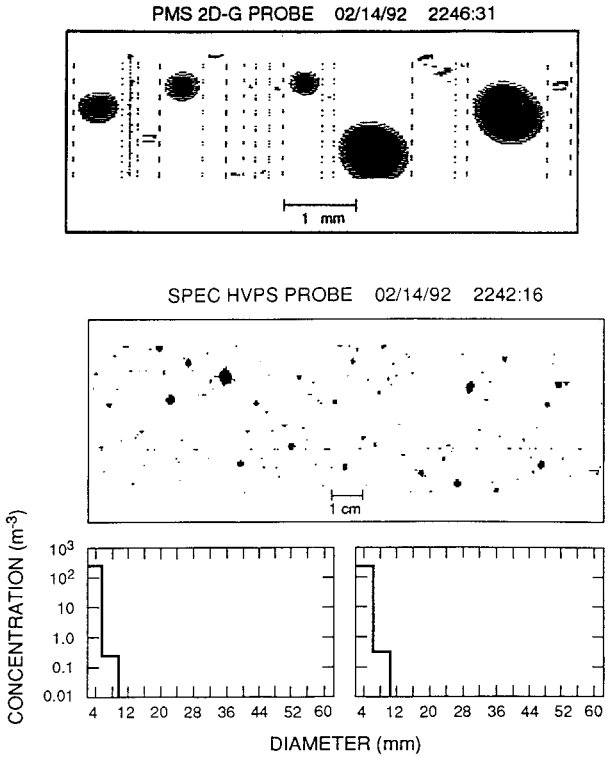

FIG. 4. Images of melted and partially melted snow particles observed at 0.6 km (+4°C) by (top) 2D-G probe and (middle) HVPS. Histograms of particle size distribution shown at the bottom are 1-km averages from two independent HVPS channels.

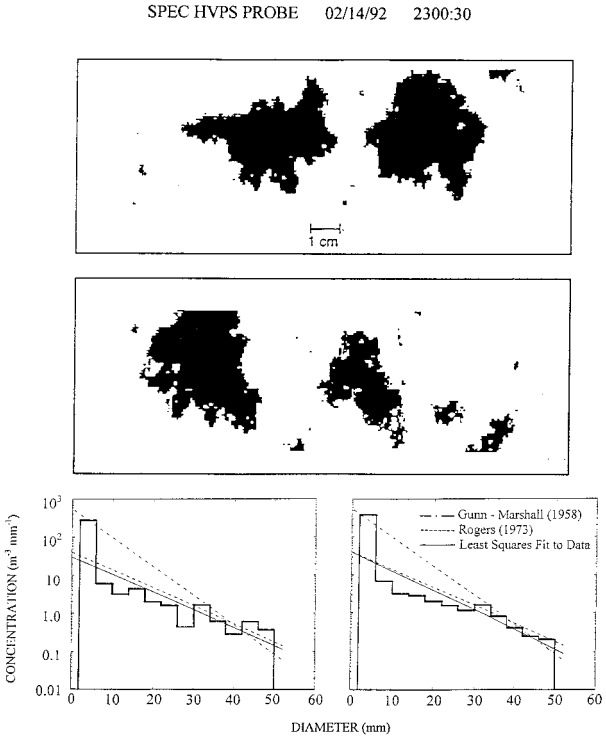

FIG. 5. Images of 4–5-cm snowflakes and 1-km averaged histograms of particle size distribution observed at 0.6 km (+1.0° C) from two independent HVPS channels compared with Gunn–Marshall (1958) parameterization for an equivalent rainrate of 9 mm h^{-1} and 5:1 ratio of unmelted to melted snowflake size, (dot-dash line) least squares fit to snowflake size distribution measurements from Rogers (1973), and (dashed line) least squares fit to HVPS data (Solid line).

The numerical model of aggregation put forth by Holroyd (1971) suggests that dendrites will aggregate faster than other types of crystals. Rogers' (1973) study showed that all seven of the events with precipitation rates >4 mm h^{-1} (up to 14 mm h^{-1}) were composed predominantly of stellar dendrites. (Figure 3 shows that dendrites were observed at −17°C in this CASP II storm.) Rogers also noted that most larger snowflakes are composed of dendrites that contain an ''origin'' ice crystal, which is typically a dendrite that is 3 mm or larger, accompanied by ''majority'' crystals, which are usually dendrites that are about 1 mm in size. Rauber (1985) also noted that aggregates observed at Steamboat Springs, Colorado, almost always contained a large (3–5 mm) dendritic ice crystal which he called a ''platform'' crystal. These observations support the hypothesis put forth here, that 3–5-mm dendrites observed in the region of weak convective instability were origin crystals for the very large snowflakes observed at the surface.

Magono and Nakamura (1965) show results of several hundred computations of snowflake density from surface measurements collected at Sapporo from 1958 to 1962. The size and density of the snowflakes were estimated by tracing the horizontal dimensions of the flakes on filter paper before and after they melted. Their results indicate that snowflake density (ρ_{SF}) varies over more than two orders of magnitude, ranging from approximately 0.004 (at 2.5) to 0.6 g cm^{-3} (at 0.3 cm). The density of snowflakes depends on several factors, including the types and sizes of the constituent ice crystals (Diamond and Lowry 1954), crystal packing, and the amount of riming (Power 1962). Holroyd (1971) sorted the data collected by Magono and Nakamura and found that the ''dry'' snow cases followed a best fit equation of $\rho_{SF} = 0.017D^{-1}$, where D in cm is the mean of the length and width of the flake. Rogers (1973) supplemented the dataset of Magono and Nakamura from his observational study in Laramie and computed a best fit equation for ''wet'' snow to be $\rho_{SF} = 0.0724D^{-1}$.

Using Rogers' (1973) equation for wet snowflakes, the largest snowflakes observed in this CASP II storm would have a density of about 0.015 g cm^{-3}. Although 4–5-cm snowflakes were observed at Torbay, the maximum dimension of the largest snowflakes captured and allowed to melt in plastic bags was about 3 cm. The equivalent melted diameter of the 3-cm snowflakes was about 0.7 cm. The observers at Torbay estimated that the flakes had a vertical height to horizontal length ratio of about 3:1, giving a snowflake density of about 0.02 g cm^{-3} for the 3-cm flakes, which is also in good general

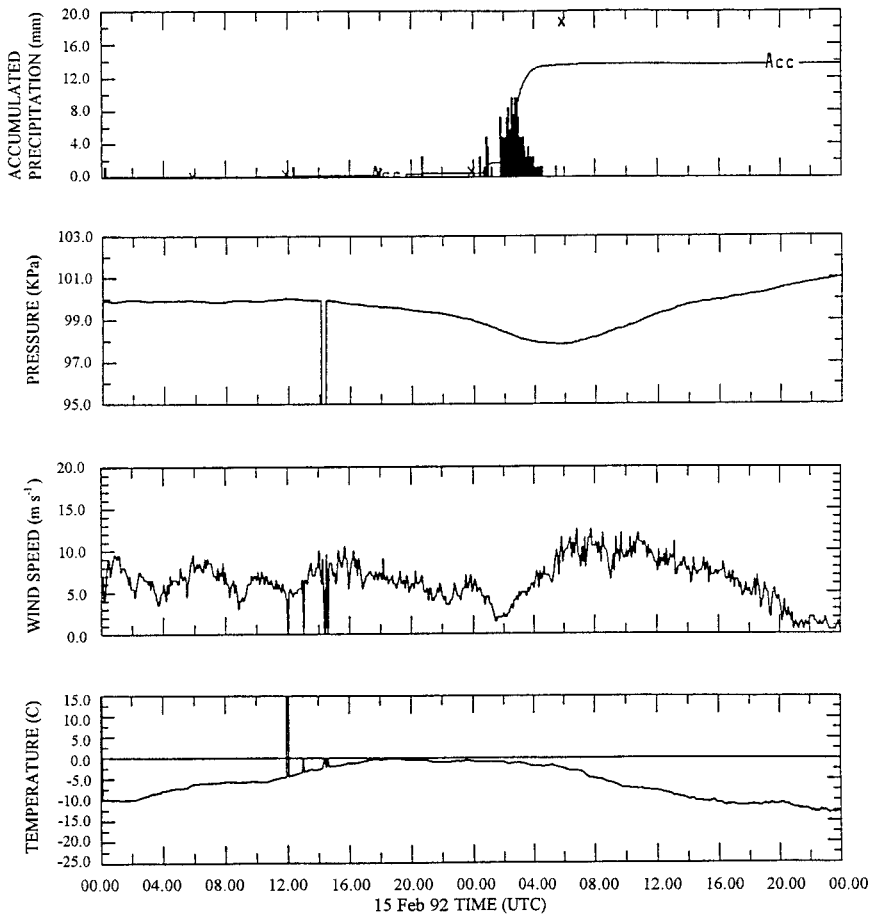

FIG. 6. Time series of surface measurements taken at the St. John's airport. The very large snowflake event occurred at about 0230 UTC.

agreement with Rogers' formula. Auer (1971) reported a melted diameter of 0.6 cm from 5-cm snowflakes captured in Laramie. He did not describe the geometry of the snowflakes, so the snowflake density cannot be determined. However, he did report particle concentrations of 4, 1, and 1 m^{-3}, for 3-, 5-, and 6-cm diameter snowflakes, respectively, which agrees well with the size distribution shown in Fig. 5.

In addition to snowflake size distributions measured by the HVPS, Fig. 5 also shows equations of the form

$$N(D) = N_0 e^{-(\lambda D)}, \tag{1}$$

where $N(D)$ is the snowflake size distribution and D is snowflake diameter. The three equations in Fig. 5 are from a least squares fit to the HVPS measurements (solid line), a least squares fit to a snowflake size distribution measured by Rogers (1973) during an event with the largest (3.5 cm) snowflake observed in his 28 cases (dashed line), and the Gunn and Marshall (1958) parameterization where $N_0 = 3800R^{-0.87}$ cm^{-1} and $\lambda = 25.5R^{-0.48}$ m^{-3} mm^{-1} and R is melted equivalent snowfall rate in mm h^{-1} (dash-dot line). A value of $R = 9$ mm h^{-1} (Fig. 6) and a ratio of 5:1 maximum snowflake dimension to equivalent melted diameter was used in the Gunn and Marshall parameterization. The comparison in Fig. 5 shows that the HVPS measurements from the CASP II storm are in good agreement with Rogers' equation for the event with the largest (3.5 cm) snowflakes he observed. The Gunn–Marshall equation has a steeper slope, which agrees better with Rogers' measurements of the size distributions of smaller snowflakes. The Gunn–Marshall parameterization is based on several empirical measurements, and in most regions of the world very large snowfall events are rare, so the ensemble Gunn–Marshall distribution may not adequately represent these events.

4. Synthesis of in situ and remote observations with models

a. Description of MM5 mesoscale model

A fifth-generation mesoscale model has been developed jointly at the Pennsylvania State University and NCAR (Anthes and Warner 1978; Anthes 1990; Grell et al. 1994). Version v1.0 was used in this work, which

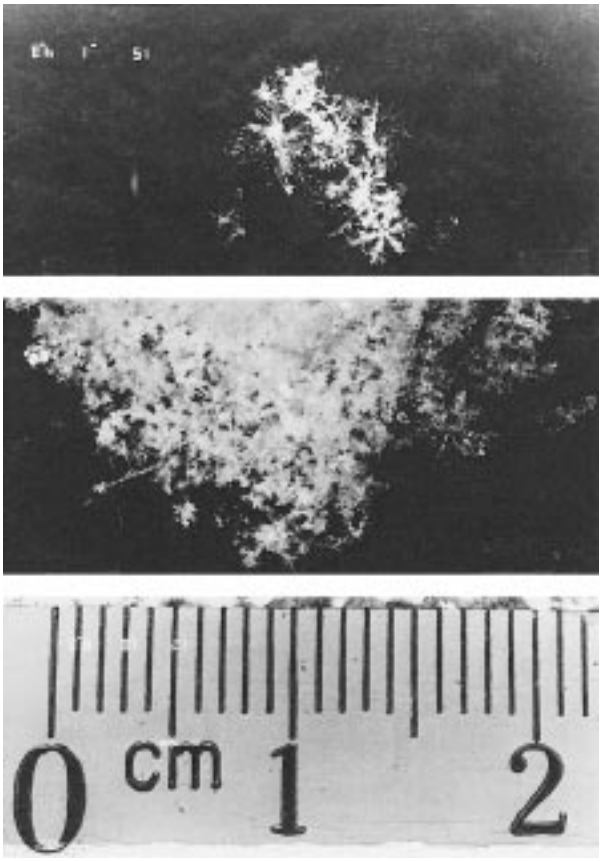

FIG. 7. Photographs of snowflakes captured at Torbay during the very large snowflake event.

is three-dimensional, nonhydrostatic with explicit moisture, and has simple mixed-phase ice physics (Dudhia 1993) with the Grell cumulus parameterization scheme (Grell 1993). The model used three nests with time-dependent lateral boundary conditions and a high-resolution planetary boundary layer. The spatial domains of the three nests with grids of 90, 30, and 10 km are shown in Fig. 8. All of the domains contained 23 levels approximately 50 mb apart. The 90- and 30-km domains were initialized at 0000 UTC and the 10-km domain was initialized at 1800 UTC on 14 February. The 30- and 10-km domains were advected along with the center of the low pressure. The 90-, 30-, and 10-km domains were all terminated at 0000 UTC 15 February. The nonhydrostatic, nested grid system allows synoptic and mesoscale forcing to be fed down into the cloud scales. Topographical, coastal, land-use, and sea temperature conditions are some of the more important features included in the model.

The microphysical scheme assumed that liquid cloud water and rain exist below the freezing level and snow and ice crystals above the freezing level. The density for rain was 1 g cm^{-3} and for snow 0.1 g cm^{-3}. For snow and rain, the Marshall–Palmer version of (1) with fixed N_0 was used, where $N_0 = 8 \times 10^6$ m^{-4}, for rain,

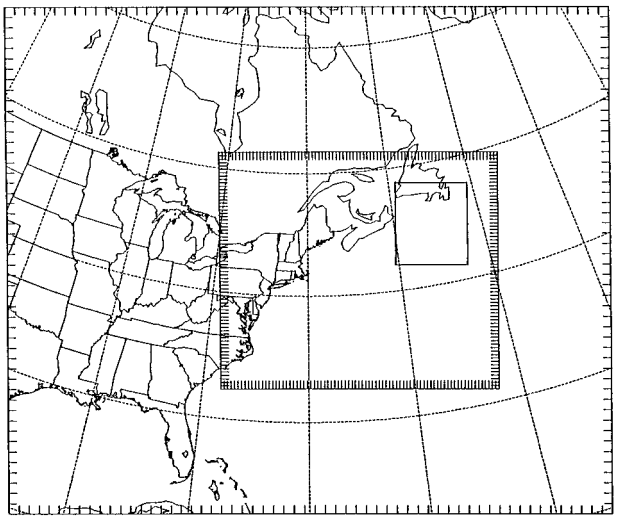

FIG. 8. Map showing spatial domains of the 90, 30, and 10 km nested grids used in the MM5 model runs.

and for snow, $N_0 = 2 \times 10^7$ m^{-4}. The slope parameter λ is represented in the model by

$$\lambda = \left(\frac{\pi N_0 a}{m}\right)^{1/4}, \tag{2}$$

where a is the particle density (g cm^{-3}) and m is the atmospheric mass content of the particles (g m^{-3}).

MM5 was run both with and without nudging. The technique included nudging on the 90-km domain toward National Meteorological Center (NMC) 3-h surface analyses and nudging toward individual observations on all three domains. In addition to the standard NMC surface observations, surface stations were included from Ontario, Quebec, the Canadian Maritimes, and Newfoundland. The standard NMC upper-air stations were supplemented with soundings from some special Canadian stations and five dropsondes launched by the aircraft.[3] All of the observations in addition to the NMC data were supplied by AES.

b. Integration of mesoscale observations and MM5 model

The results from MM5 were compared with the analysis of surface and upper-air observations and with SSM/I satellite observations to assess the ability of the model to reproduce features on both the synoptic- and the mesoscale. The primary goal of this work is to un-

[3] Dropsonde measurements were incorporated here for the first time into the MM5 model. A data point is transmitted from the sonde every 10 s and the sonde falls at about 9 m s^{-1}, so it is not possible to measure the exact pressure when the sonde plunges into the sea. The MM5 model surface pressure, temperature, and dewpoint temperature were used at the sea surface.

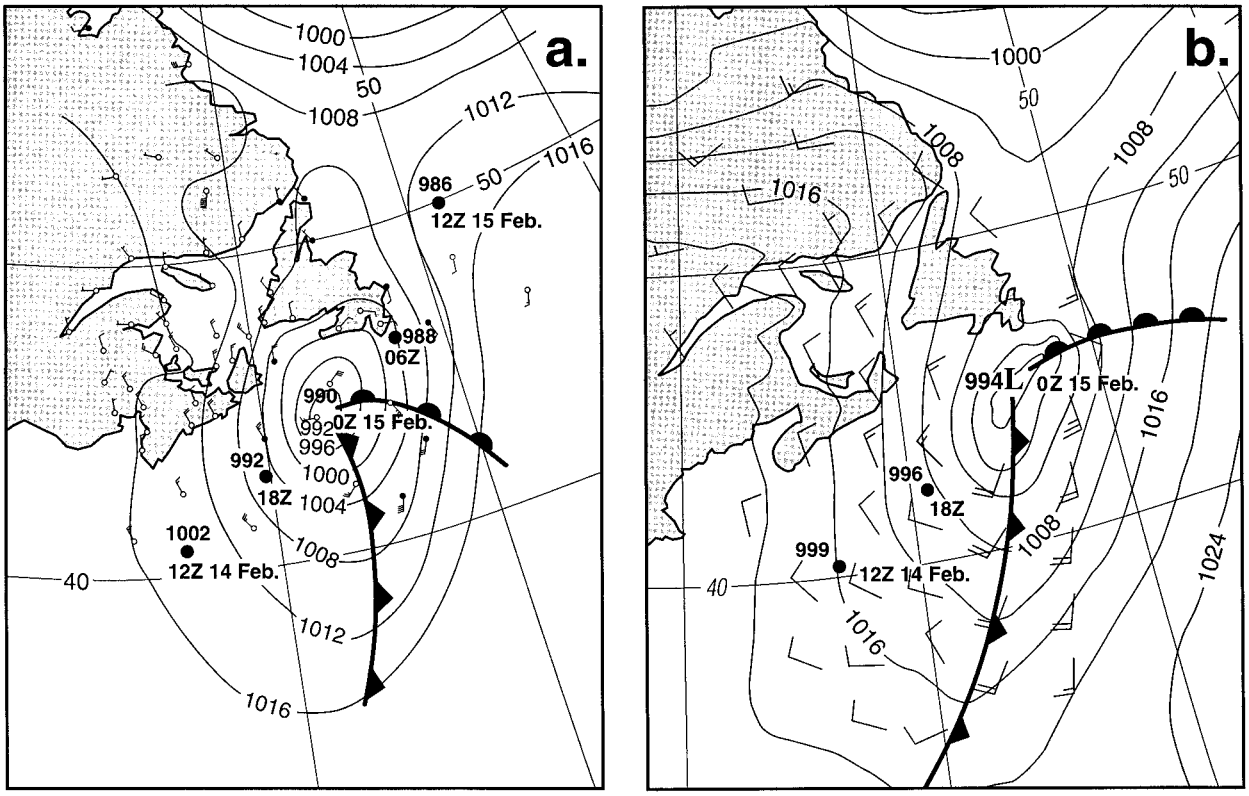

FIG. 9. Comparison of 0000 UTC 15 February 1995 surface analyses from (a) AES Newfoundland Weather Center and (b) MM5 model prediction. The solid circles show positions and magnitude of the centers of low pressure in 6-h intervals.

derstand the origin and development of the very large snowflakes. In order to utilize model results on the cloud scale, it is necessary to check and verify the ability of the model to faithfully reproduce the critical mesoscale features.

Figure 9 shows a comparison of 24-h movement of the centers of low pressure and surfaces analyses at 0000 UTC, about 1 h after the time the very large snowflake event was observed by the aircraft. The position of the low predicted by the model consistently lags the actual low pressure center by about 80 km.[4] The comparison of the simulated surface analysis from the 10-km domain and the analysis based on observations at 0000 UTC is very good. The analysis is done from sparse measurements over the ocean so that the actual shape of the isobars is uncertain. Figure 9 shows that over the coastal region, the agreement in the isobars and wind barbs between the model and analysis is excellent. This comparison helps to establish the validity of MM5 in simulating the dynamics on the meso-α scale (200–2000 km) at the time of the very large snowflake event.

Figure 10 shows a comparison between the MM5 predicted precipitable water field, microphysical data derived from the 85-GHz channel of the SSM/I satellite and the 11-μm channel of the Advanced Very High Resolution Radiometer (AVHRR) on the *NOAA-12* satellite. The SSM/I observations, analyzed by Schols et al. (1998), suggest that a line of convection containing graupel particles extends for hundreds of kilometers south of the center of low pressure. The position and aspect ratio of this line is in good agreement with a band of precipitable water predicted by MM5 on the 30-km domain. The θ_e and vertical velocity fields generated by the model (not shown) support the observation that this was convective precipitation. The comparison between satellite and model results seen in Fig. 10 is very good and supports the ability of MM5 to predict features on the meso-α scale and also the meso-β (20–200 km) scale.

The good agreement in MM5 results and observations seen on the meso-α and meso-β scales suggests that comparisons on finer scales may be justified. Figure 11 shows comparisons of vertical cross sections of temperature and θ_e derived from 1) MM5 model results

[4] The model predicts a slightly slower (by about 4.5 h) development of the storm than shown by the AES analyses. Since here we are using MM5 for analysis instead of as a predictive tool, all model times given in this paper have been time-adjusted to establish consistency with the observations. This was accomplished by using the model product that occurred either 4 or 5 h later in time, depending on which product appeared to better fit the observational analyses.

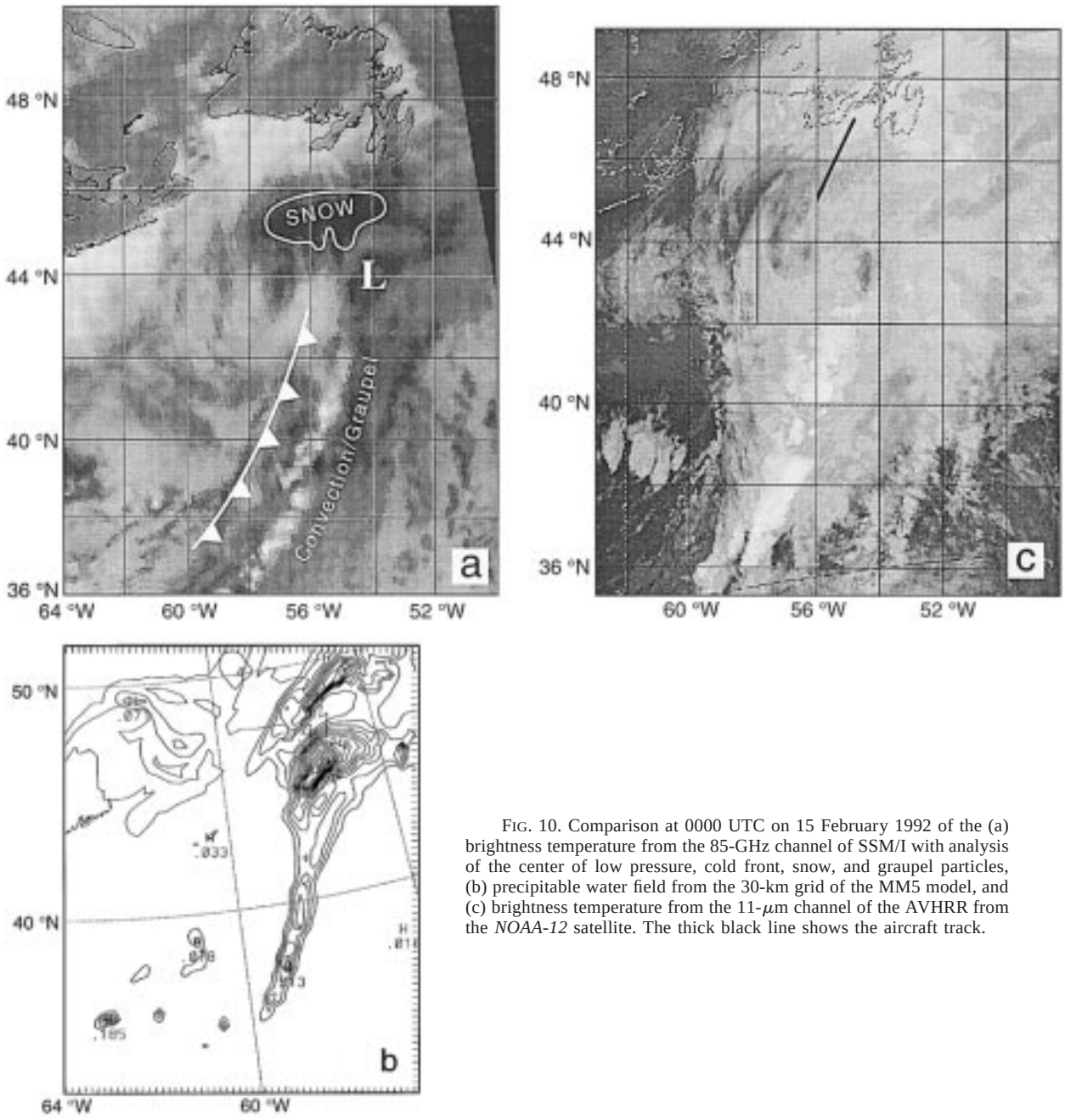

FIG. 10. Comparison at 0000 UTC on 15 February 1992 of the (a) brightness temperature from the 85-GHz channel of SSM/I with analysis of the center of low pressure, cold front, snow, and graupel particles, (b) precipitable water field from the 30-km grid of the MM5 model, and (c) brightness temperature from the 11-μm channel of the AVHRR from the *NOAA-12* satellite. The thick black line shows the aircraft track.

without 4DDA and nudging toward dropsonde observations, 2) model results with 4DDA and nudging, and 3) only aircraft dropsonde measurements. Again, the agreement between the in situ observations and model results is remarkably good, particularly considering that the model was started 26 h in advance. The model results demonstrate that the (sloping) trends in both the isotherms and lines of constant θ_e are well represented by the physics of the model alone, without 4DDA and nudging. The 4DDA and nudging only adjust the contours slightly toward those of the observations.

In the observational study of this case, Lawson et al. (1993a) suggest that the development of the 14 February very large snowflakes was linked with 1) weak convective instability at an altitude of 5 km that supported development of large dendritic origin crystals of the type found later about 200 km downwind in the very large snowflakes, and 2) a thick (~600 m), nearly isothermal layer near 0°C that sloped downward along the fall direction of the origin crystals/snowflakes. Both these factors are very consistent with the expanded set of observations discussed in this section. The aircraft

observations in Fig. 11 show a region where $d\theta_e/dz$ is slightly negative, implying weak convective instability existed aloft near the southwest end of the aircraft track. The model results in Fig. 11 show a region aloft in the exact same location as the aircraft observations where the trend in the θ_e contours is very similar and $d\theta_e/dz$ is slightly positive. The contours of θ_e derived from the observations and the model results both slope upward at about a 30° angle and the isotherms both slope downward at about a 15° angle. The main difference in the thermal fields derived from the observations and the model results occurs below 1500 m. In this region, the model predicts much smoother contours of both temperature and θ_e than seen in the observations. The model shows a sloping isothermal layer near the 0° isotherm; however, the isothermal layer predicted by the model is not nearly as thick as seen in the measurements. Thick layers near 0°C are physically linked to a melting process operating within saturated conditions (Stewart 1984; Stewart et al. 1984). MM5 accounts for phase transitions, and, in this case, tends to make the appropriate kinematic adjustments but falls short of reproducing the fine structure below 1500 m. The agreement between the overall trends in the vertical cross sections of temperature and θ_e from the dropsonde measurements and the MM5 model results is very good. This suggests that at least some aspects of the model results reproduce the general trends seen in the observations on even the mesoγ scale (2–20 km).

The very good agreement between the observations and the model in Figs. 9–11 encourages us to judiciously use the model results to expand (temporally and spatially) the limited in situ aircraft observations. Thus, MM5 is used here as a data analysis tool, instead of a forecast tool.

The weak convective instability aloft (Fig. 11) was directly associated with the presence of 3–5-mm dendritic ice crystals (Figs. 2 and 3). MM5 model results in Fig. 12 show that the convective instability at 545 mb was directly above a region between 850 and 700 mb that is about 50 km in diameter and exhibits strong counter-clockwise circulation (i.e., convergence). The localized convergence at the lower level is at the northern end of the long line of convection observed by satellite (Fig. 10) and was generated along the frontal boundary between the cold and warm sectors. This strongly suggests that the observations of supercooled liquid water and dendrites at −17°C were supported by convection generated by convergence in the lower levels. The MM5 500-mb wind field, also shown in Fig. 12, indicates that there was no convergence *at* the level where the dendrites were observed. Instead, at 545 mb the MM5 wind data, supported by the in situ observations from the Convair air motion system, show a uniform field of southwest winds with velocities of 20–25 m s^{-1}. Thus, the dendritic crystals observed at 545 mb were probably transported rapidly northeastward in the strongly sheared flow from the southwest.

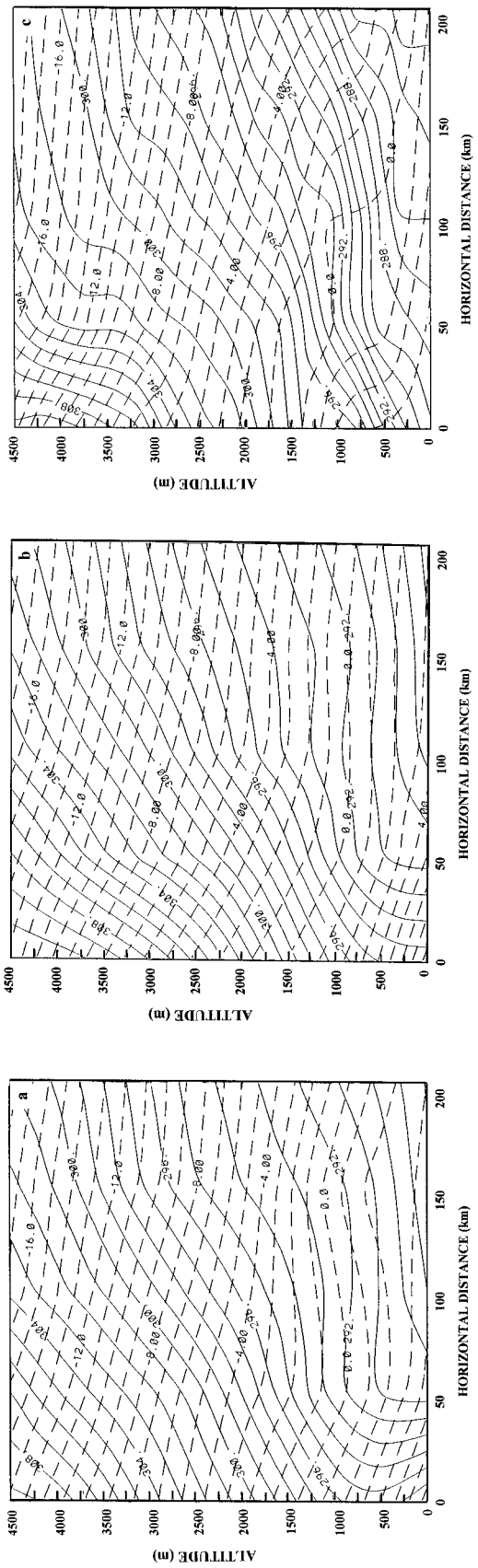

FIG. 11. Vertical cross sections showing isotherms (dashed lines) and θ_e (solid lines) along the aircraft track at 2100 UTC computed using (a) MM5 model results initialized 26 h previously, (b) MM5 model results with 4DDA and nudging, and (c) analysis of five dropsondes released between 2002 and 2050 UTC.

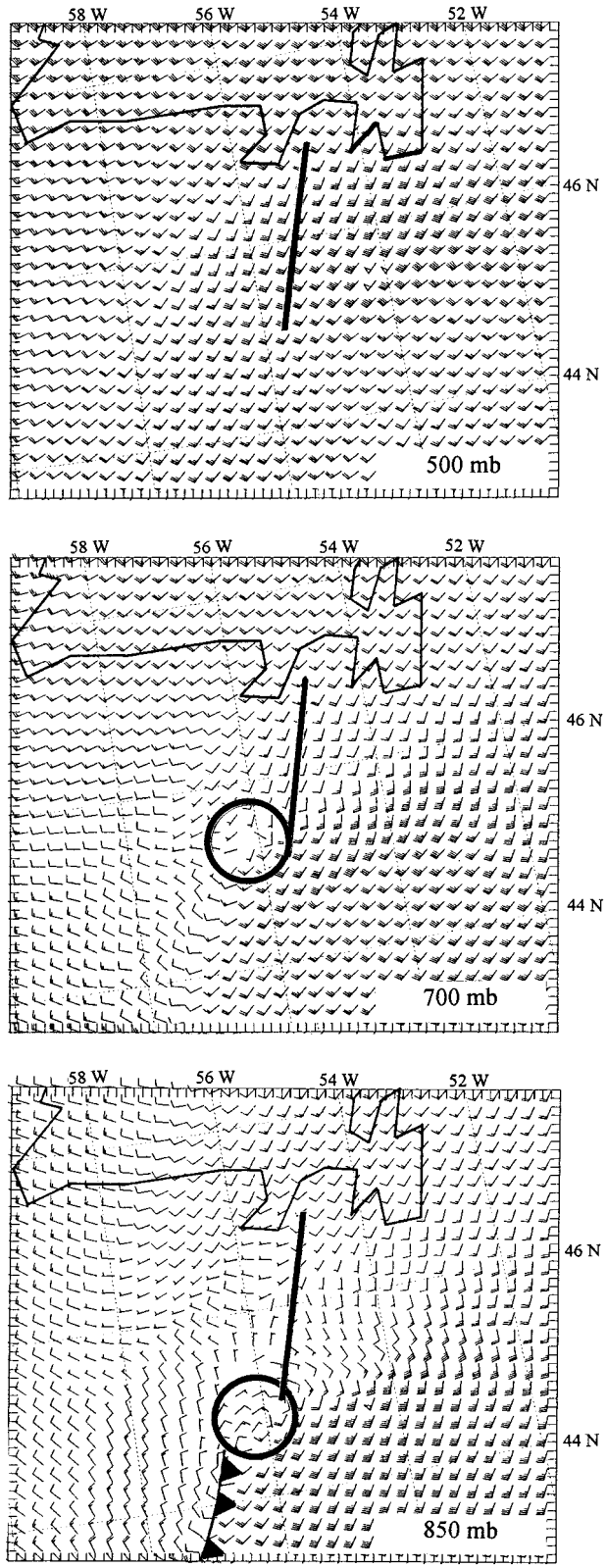

FIG. 12. MM5 model results at 2100 UTC showing wind fields at 850, 700, and 500 mb. The heavy solid line is the aircraft flight track and the circles at 850 and 700 mb highlight regions of counter-clockwise circulation (i.e., convergence and vertical air motion) beneath a strong southwesterly flow at 500 mb.

The observations of large snowflakes taken on the ground showed that they were mainly composed of millimeter-sized dendritic crystals and needles (Fig. 7); such dendritic particles were only observed aloft upwind of the airborne observations of very large snowflakes. Thus, it is reasonable to suggest that the dendrites were associated with the development of the very large snowflakes. The very large snowflakes were observed about 2.3 h and 130 km downwind of the airborne observations of dendrites aloft, which is consistent with a mean transport velocity of about 15 m s^{-1}. This implies that the hydrometeors had an average fall velocity of about 0.5 m s^{-1}, which is reasonable for a large dendritic ice crystal (Pruppacher and Klett 1978), but is too small for the large snowflakes. Magono and Nakamura (1965) show that the fall velocity is largely a function of snowflake density and that very large snowflakes with a density of 0.02 g cm^{-3} fall at about 2–3 m s^{-1}. Auer (1971) measured the fall velocity of very large snowflakes at 700 mb to be about 2–3 m s^{-1} and this is consistent with measurements made by one of the authors (RPL) in Boulder, Colorado, at 850 mb. Thus, simple computations using published fall velocities substantiated by our measurements suggest that the snowflakes would fall short of the observed location unless there were vertical air motions that effectively reduced the particle fall velocity.

The MM5 model wind fields shown at 2100 UTC in Fig. 12 do not reveal any areas of low-level convergence (producing vertical air motion) downwind of the location of the dendrites observed aloft. However, the model wind fields at 700 mb 1 h later (2200 UTC) and at 850 mb 2 h later (2300 UTC) seen in Fig. 13 show areas of low-level convergence about 50 km in diameter that coincide with the observed location of the large snowflakes. The associated vertical air motion would effectively retard the fall velocity of the particles. Figure 14 shows cross sections of the vertical air motion fields computed by MM5 along the aircraft track at 2200 UTC, suggesting that upward vertical velocity maximums of about 0.2–0.4 m s^{-1} were associated with the locations of low-level convergence seen in Fig. 13. The presence of widespread ascent near the warm front is certainly expected. In addition, the fact that this ascent was also occurring near 0°C is quite consistent with the predictions of Szeto et al. (1988a,b) and Szeto and Stewart (1997). They showed that in a baroclinic environment, an organized mesoscale circulation should result from horizontal variations in the diabatic process of melting and other associated processes such as sublimation and evaporation.

In support of the model results, a time–height vertical cross section of Doppler radar measurements from the UT radar (taken later when the very large snowflake event was over St. John's) are also shown in Fig. 14. Based on Doppler radar measurements of the convergence–divergence field, vertical (air) velocities of 0.1–

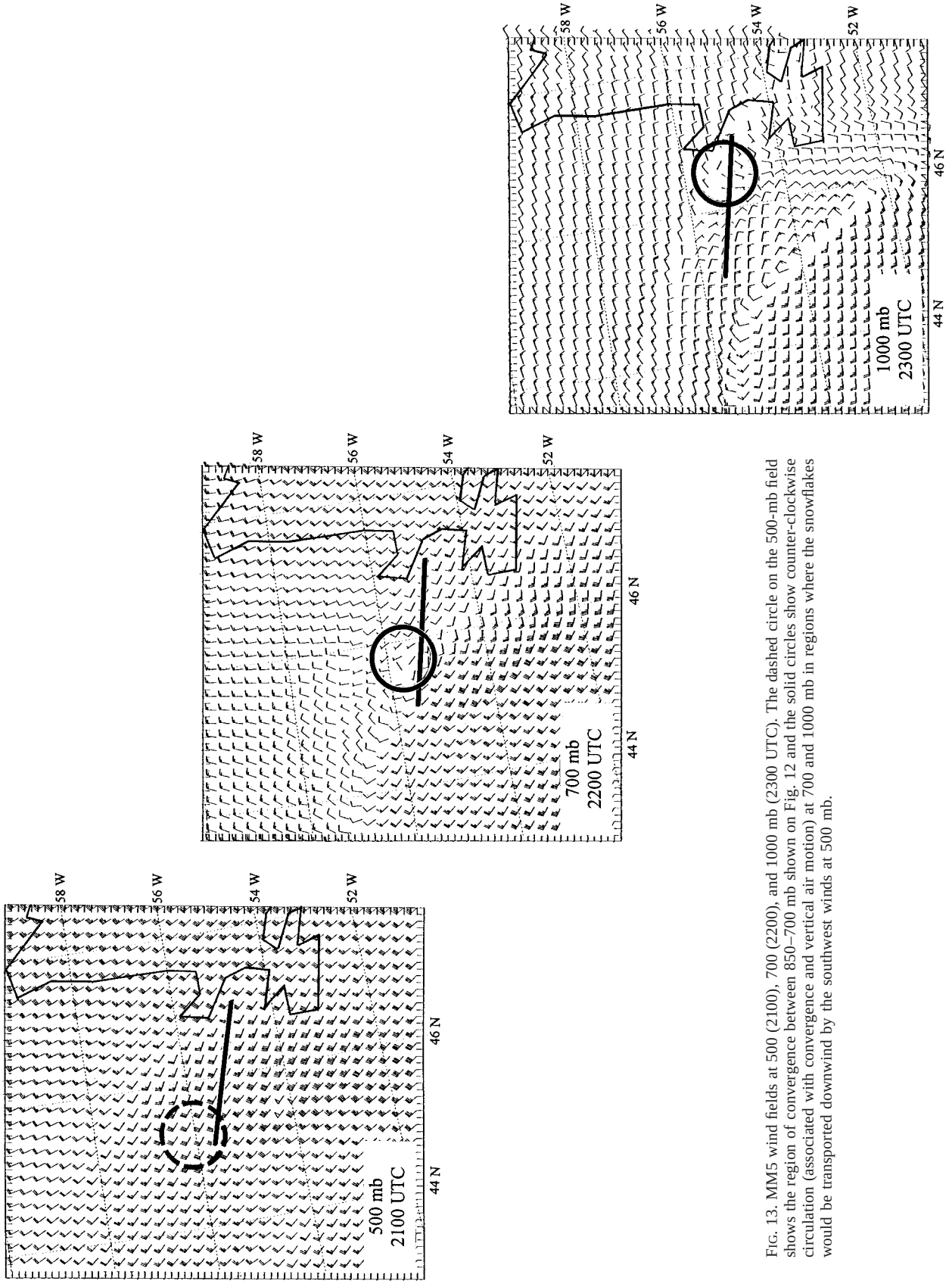

FIG. 13. MM5 wind fields at 500 (2100), 700 (2200), and 1000 mb (2300 UTC). The dashed circle on the 500-mb field shows the region of convergence between 850–700 mb shown on Fig. 12 and the solid circles show counter-clockwise circulation (associated with convergence and vertical air motion) at 700 and 1000 mb in regions where the snowflakes would be transported downwind by the southwest winds at 500 mb.

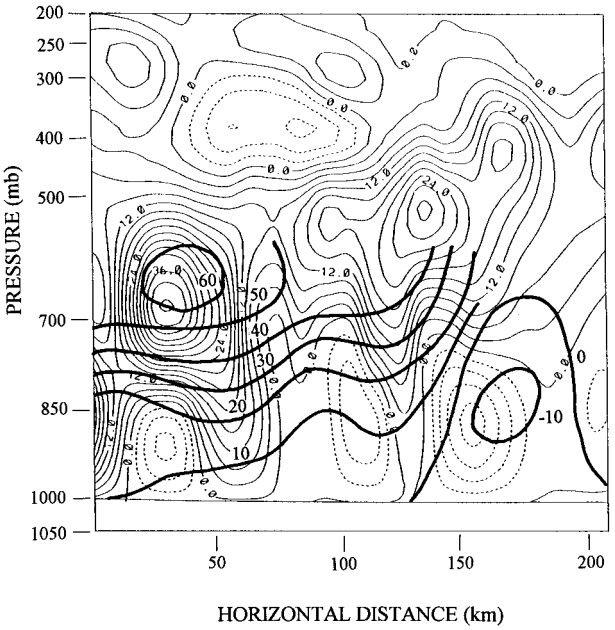

FIG. 14. MM5 vertical cross section along aircraft track of vertical velocity field at 2200 UTC where solid lines are upward and dashed lines are downward velocities (cm s^{-1}). Bold lines superimposed over MM5 product are vertical velocity contours (bold labels in cm s^{-1}) from UT Doppler radar when the very large snowflake event occurred at Torbay. The horizontal scale for the radar data was translated from time to distance using the observed motion of the storm.

0.6 m s^{-1} are computed in the region where the snowflakes were observed.

The combination of MM5 results and Doppler radar observations strongly suggests there was convergence and upward vertical velocities in the region of 850–500 mb along the path over which the very large snowflakes developed or were occurring. The resulting vertical air motions would have effectively slowed the fall of the hydrometeors so that observations of the location of the very large snowflakes are consistent with measurements of fall velocities reported in the literature.

c. Microphysical observations and model results

Aircraft, radar, and satellite observations, integrated with the MM5 model run in 4DDA mode, are all consistent with the concept that the storm environment was favorable for the very rapid aggregation of dendritic (and other) ice crystals into 4–5-cm snowflakes. The nature of the processes responsible for this can be examined in detail.

Figure 15 shows the maximum 1-km averaged measurements of IWC, LWC, and maximum particle dimension (D_{max}) as a function of altitude, as well as the horizontal distribution of IWC and D_{max} through the plume of very large snowflakes. In Fig. 15, vertical profiles of LWC and D_{max} measurements are interpolated linearly and the IWC is fit with a spline. The maximum dimension of the snowflakes increased from 3–5 mm at 5 km to 1–3 cm at 1.2 km and then to 4–5 cm at 0.6 km. The equivalent IWC was computed from the particle size distribution shown in Fig. 5 and Rogers' (1973) equation for wet snowflake density. The uncertainties in computing IWC from particle imaging probes may be a factor of 2 (Heymsfield 1986), or even much larger, depending on the geometry and density of the snowflakes and assumptions made in the computations. However, the maximum 1-km average IWC computed from the particle images is 1.8 g m^{-3} a 1-s peak of 2.7 g m^{-3}, which are very high values in winter storms (for example, see Rogers 1973). An independent analysis of IWC derived from SSM/I satellite measurements by Schols et al. (1998) is also shown in Fig. 15. The IWC derived from the SSM/I measurements also increases rapidly from 3 km downward to 1 km, showing a peak value of 2.6 g m^{-3} at about 1 km. The composite aircraft measurements shown in Fig. 15 suggest that a moderate increase in IWC occurred between 4.9 and 3.6 km, a commensurate decrease occurred from 3.6 to 2.2 km, and then a dramatic increase in IWC took place (from about 0.16 to 1.8 g m^{-3}) between 2.2 and 0.6 km.

The two microphysical mechanisms that are generally considered to be responsible for a net gain in ice particle mass concentration are growth by vapor diffusion and accretion of supercooled drops. Aggregation of ice particles, on the other hand, increases the mass of some particles at the expense of other particles (within a specific volume). This has the effect of shifting the median of the ice particle size distribution toward the larger sizes and decreasing the total number concentration. Aggregation can, however, increase the total mass concentration at a specific locale if larger ice particles aloft fall down through a field of smaller snowflakes suspended in an updraft. In the remainder of this section, we address the contributions of particle mass growth by accretion and diffusion and the possibility of ice particles growing rapidly via sedimentation and aggregation.

The measurements in Fig. 15 indicate that the supercooled LWC available for conversion to ice is small, on the order of 0.05–0.2 g m^{-3}. This suggests that accretion is not sufficient to account for the rapid increase in IWC. However, radar measurements and MM5 simulations indicate that the particles fell through a region where the upward vertical velocity was on the order of 0.5 m s^{-1} and the atmosphere was saturated, so that a continuous replenishment of available supercooled cloud water would have occurred. A simple calculation shows that if a vertical air velocity of 0.5 m s^{-1} persisted for 3000 s at the observed temperature and pressure, the adiabatic LWC would be on the order of 1.5 g m^{-3}, which would account for the observed increase in particle mass concentration. It is also known, however, that the rate of accretional growth is a strong function of the available supercooled LWC. For example, Cooper and Lawson (1984) show that LWC appears as an exponent in the equation for accretional growth, and that the ac-

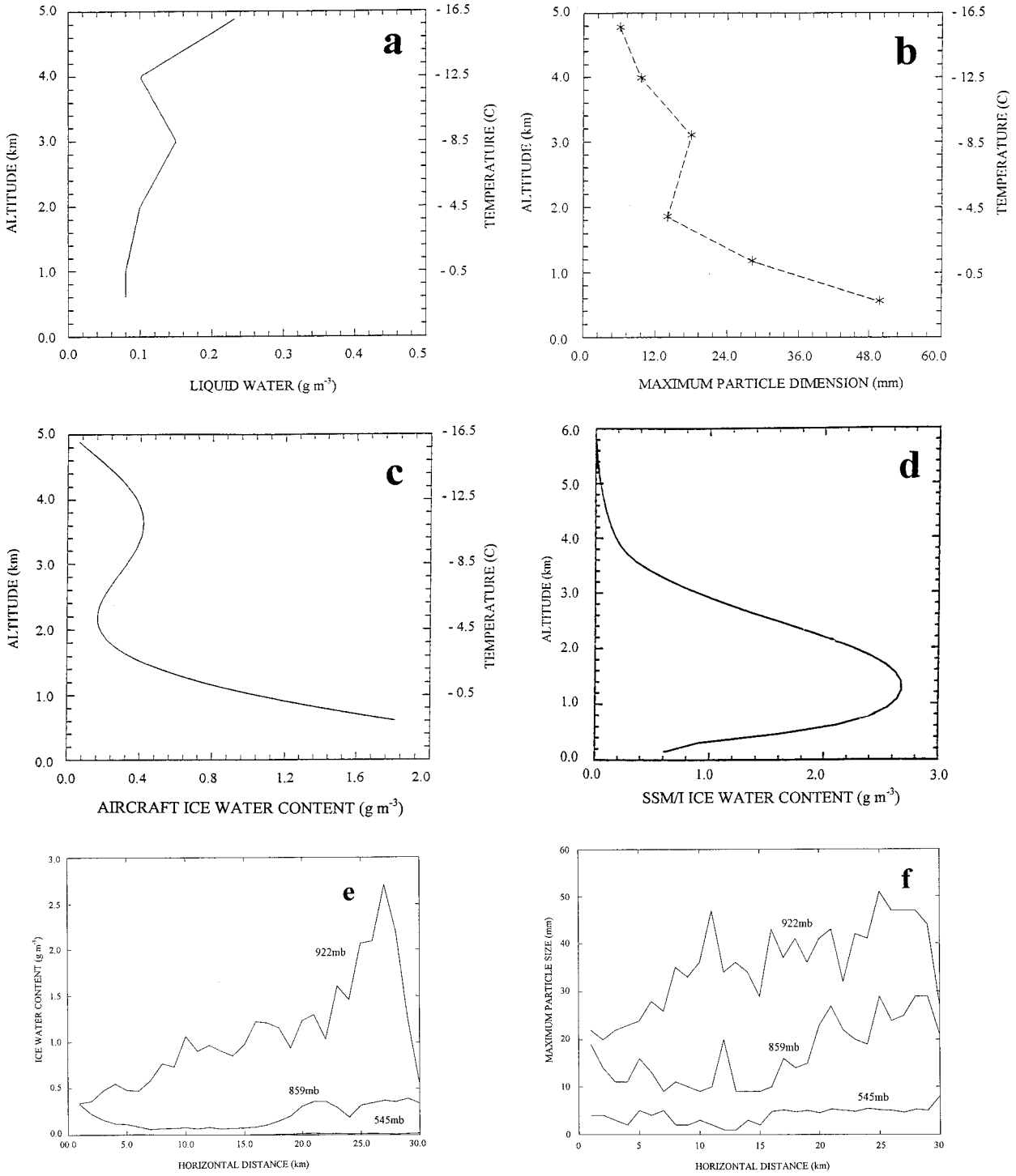

FIG. 15. Aircraft observations of vertical profiles of (a) liquid water content, (b) maximum particle dimension, and (c) 10-s averaged ice water content. A vertical profile of ice water content derived from SSM/I satellite measurements and adapted from Schols et al. (1998) is shown in (d). The horizontal distribution of 1-s point measurements of (e) ice water content and (f) maximum particle dimension from aircraft measurements within the plume of very large snowflakes are also shown for three pressure levels.

cretion rate expected for LWC ~ 0.2 g m^{-3} is too slow to produce the observed increase in particle mass. Also, observations made in summer cumulus by Cooper and Lawson (1984) show that aggregation (instead of accretion and graupel formation) predominates when the LWC $\lesssim 0.5$ g m^{-3}. The large snowflakes observed at the ground (Fig. 7) showed evidence of light riming, not the heavy riming expected from high LWC. Thus, conditions were adequate to support some collection of supercooled cloud water; however, accretional growth did not account for the observed increase in particle mass concentration.

Particle growth by diffusion is also a candidate for explaining the rapid increase in IWC from 2.2 to 0.6 km seen in Fig. 15. While theory and laboratory observations of the diffusional growth rates of individual ice crystals agree relatively well (Pruppacher and Klett 1978), little is known about the effective diffusional growth rate of aggregates of ice crystals. This is mainly due to a lack of theoretical and observational methods for determining the effective ventilation factor of aggregates. That is, should the diffusional growth rate of an aggregate be treated like the sum of the (ventilated) individual crystals falling at the terminal velocity of the aggregate, or more like the growth rate of a single large crystal? While the actual diffusional growth rate probably falls somewhere in between, it is worthwhile here to explore the maximum possible growth rate using theory as a guideline. Pruppacher and Klett (1978) show that the maximum diffusional growth rate for ice crystals at -5°C is about 10^{-8}g s^{-1}. Next, assume that the falling aggregates are full of thousands of ''ventilation holes,'' so that the ice crystal concentration is effectively multiplied by four orders of magnitude[5], producing an effective particle concentration on the order of 10^3–10^4 m^{-3}. Finally, if we assume that the particle velocity of the large aggregates falling from 2.2 to 0.6 km is reduced by upward vertical air motion to 0.5 m s^{-1}, then the time for diffusional growth is on the order of 3000 s. Multiplying these numbers together gives an increase in IWC of 0.03 g m^{-3}, which is still far less than the observed value of 1.6 g m^{-3}. This simple calculation suggests that the observed dramatic increase in IWC from 2.2 to 0.6 km is also not explainable solely by diffusional growth.

Next, we address the possibility that the very large snowflakes and high IWC were the result of aggregation of larger ice particles falling into a field of smaller ice particles sustained by upward vertical motion. The observations and discussion in the previous section (cf. Figs. 2 and 12–14) argue for a scenario where 1–5 mm dendrites were rapidly transported northeastward by the strongly sheared flow aloft. The larger (3–5 mm) dendrites then served the function of origin crystals (Rogers 1973) and descended into a region containing predominantly needles and smaller dendrites. Rogers (1973) observed unstable fall behavior for dendritic ice crystals larger than about 3 mm. He estimated that crystals larger than 5 mm can experience about a five-fold enhancement in collision frequency due to unstable fall behavior. In addition, local convergence in this region produced upward vertical air motion on the order of 0.1–0.6 m s^{-1} which acted to suspend the ambient field of ice crystals and prolong the interaction with the origin crystals. The rapid increase in particle size observed between 2.2 and 0.6 km (Fig. 15) corresponds with a region where the isotherms slope downward in the direction of travel of the snowflakes. Thus, the particles experienced a relatively long ($\sim$3000 s) period of exposure in the temperature region from $-5°$ to $+1$°C, a region which has classically been found to be very favorable for rapid aggregation and development of large snowflakes (Dobrowolski 1903; Magono 1953, 1960; Hobbs et al. 1974; Rogers 1973).

The Doppler radar data and MM5 model results (Figs. 13 and 14) suggest that the large dendritic origin crystals fell through a region where there was an upward vertical motion of about 0.5 m s^{-1}. The MM5 results also suggest that this vertical motion would provide upward forcing for establishment of an ambient snow field through which the larger dendrites would fall through. In this region of Canada in which the environmental temperatures often range at the surface from $-3° \rightarrow -7$°C, needles are typical and aggregates of needles are common (Stewart et al. 1990). Lo and Passarelli (1982) and Lo (1983), however, found that the slope parameter λ will not decrease past a value of about 1000 m^{-1}. They argue, based on observations (Lo and Passarelli 1981), that the limit is due to an equilibrium between the production of small particles due to breakup and large particles resulting from aggregation. Observations of the largest snowflakes (Fig. 5) suggest $\lambda \approx 100$ m^{-1}, which is considerably less than 1000 m^{-1}, the limit suggested by Lo and Passarelli (1982). A value of $\lambda \approx 100$ m^{-1}, however, is consistent with observations made by Rogers (1973), as shown in Fig. 5. Sedimentation of the larger dendritic crystals into a region with upward vertical motion comparable to the snowflake fall velocities may have created an ''accumulation zone.'' Rapid aggregation without particle breakup in association with the accumulation zone is a possible explanation for much of the explosive growth in particle size between 2.2 and 0.6 km (Fig. 15).

d. One-dimensional (1D) microphysical model analysis

The ice particle growth process was examined further by using an analytical–numerical 1D model that incor-

[5] There is no way of knowing the actual ventilation factor of a very large snowflake. A maximum enhancement of 10^4 was chosen because, in the absence of aggregation, this would produce an ice crystal concentration of about 10^3–10^4 m^3 of 2-mm crystals, which is a reasonable maximum.

porates diffusional and accretional particle growth with particle aggregation (Mitchell 1988, 1990, 1994, 1995). A fundamental assumption of the Mitchell model is that the snow size distribution can be described by the relationship

$$N(D)\, dD = N_0 D^{\nu} e^{(-\lambda D)}\, dD. \quad (3)$$

The equation for the slope parameter $\lambda(z)$ is height-dependent and includes terms for vapor diffusion, accretion of supercooled cloud water, and aggregation of ice and snow particles. It is computed by parameterizing the quantities in the first and second moments of the mass conservation equations (Mitchell 1988, 1991). This produces a differential equation that incorporates measurable quantities such as ambient temperature, IWC, and updraft speed, as well as temperature-dependent parameters drawn from the literature, such as crystal habit, collection efficiency of cloud drops, and aggregation efficiency of ice particles. The temperature dependence of drop collection and aggregation efficiencies, however, only appears indirectly through crystal habits and the calculation of fall velocities. This is unlike some other treatments of aggregation, where the collection efficiency is parameterized directly as a function of temperature. Strictly speaking, the Mitchell model is not time-dependent (although it does use fall speed and updraft velocity). The differential equation for $d\lambda/dz$ is a Bernoulli-type equation and is solved numerically in height steps (Mitchell 1988, 1990). The exponent ν governs the shape of the particle size spectra. That is, $\nu = 0$ yields exponential spectra, $\nu < 0$ gives super-exponential spectra, and $\nu > 0$ produces subexponential spectra (Mitchell 1991).

For this CASP II case, the Mitchell model was run with $\nu = 0.3$ using a dendritic crystal habit with an aggregation efficiency equal to 1. The measured temperature profile, IWC, and LWC from the aircraft measurements along with the MM5 vertical velocity were used as inputs. The main reason for choosing the Mitchell model was to assess conditions that would lead to results consistent with observations of particle growth. The mass concentration equations in the model are constrained by the measured IWC, so ice particle size distribution must satisfy the observed IWC. Particle breakup, controlled by limits on λ, may play a large role in determining the resulting particle size distribution in the mid-to-lower cloud.

Figure 16 shows a comparison of aircraft and ground observations with vertical profiles of model results for the 14 February 1992 storm. The dashed lines in Fig. 16 are aircraft observations taken in the 14 February 1990 upslope storm along the Front Range of Colorado during the Winter Icing and Storms Project (WISP) (Mitchell 1995). The WISP observations are shown only to emphasize the significant difference in microphysical measurements between typical Colorado upslope storms and the very large snowflake event observed during CASP II. In Fig. 16, there is good general agreement between the aircraft observations, ground observation, and the Mitchell model results.

The results of the Mitchell model shown in Fig. 16 suggest that the very large snowflakes cannot be produced by diffusional and accretional growth without aggregation. The model results are in general agreement with the lightly rimed, large aggregates that were observed on the ground (Fig. 7) and discussed in the previous section. In addition, at temperatures warmer than about -3°C, the model suggests that particle breakup must be inhibited in order to support the development of very large snowflakes. In this region, Fig. 16 shows that λ decreases from about 240 to 75 m^{-1} and D_{max} increases from about 2 to 4.5 cm while the particle concentration remains essentially constant. These results differ from results reported by Lo and Passarelli (1982), where particle breakup was observed to limit λ to 1000 m^{-1}. Here, the combined results of the observations and Mitchell model suggest that in this CASP II storm particle breakup limits λ to about 210 m^{-1} at temperatures < -3°C. At temperatures > -3°C, aggregation was very active, the very large snowflakes formed, and particle breakup appeared to be absent (or inhibited). Furukawa et al. (1987) demonstrated in the laboratory that a quasi-liquid layer forms on hexagonal columns at temperature ≥ -4°C and on plates at temperature ≥ -2°C. (No tests were conducted on needles and dendrites.) By producing stickier crystals, a quasi-liquid layer may help explain the inhibition of particle breakup in the CASP II storm at temperature ≥ -3°C.

5. Discussion and concluding remarks

Aircraft observations (summarized here and discussed by Lawson et al. 1993a) strongly suggest that a region of weak convective instability aloft generated large (3–5 mm) dendrites that were transported downward and fell into a downward-sloping near 0°C layer where the dendrites and existing needles aggregated rapidly into very large (4–5 cm) snowflakes. In this work we incorporated aircraft, radar, surface, and satellite observations with output from a nested mesoscale model (MM5) run in the four dimensional data assimilation (4DDA) mode to enhance our understanding of the processes leading to development of the very large snowflakes. In addition, the Mitchell numerical–analytical model was used to help understand the microphysical processes leading to the development of very large snowflakes.

There was good agreement between the observational and the MM5 model results on mesoα, mesoβ, and mesoγ scales. Some examples are given below to illustrate the extent of the comparison and to provide the justification for judiciously extrapolating the observations both temporally and spatially:

1) The model accurately simulated the position of the

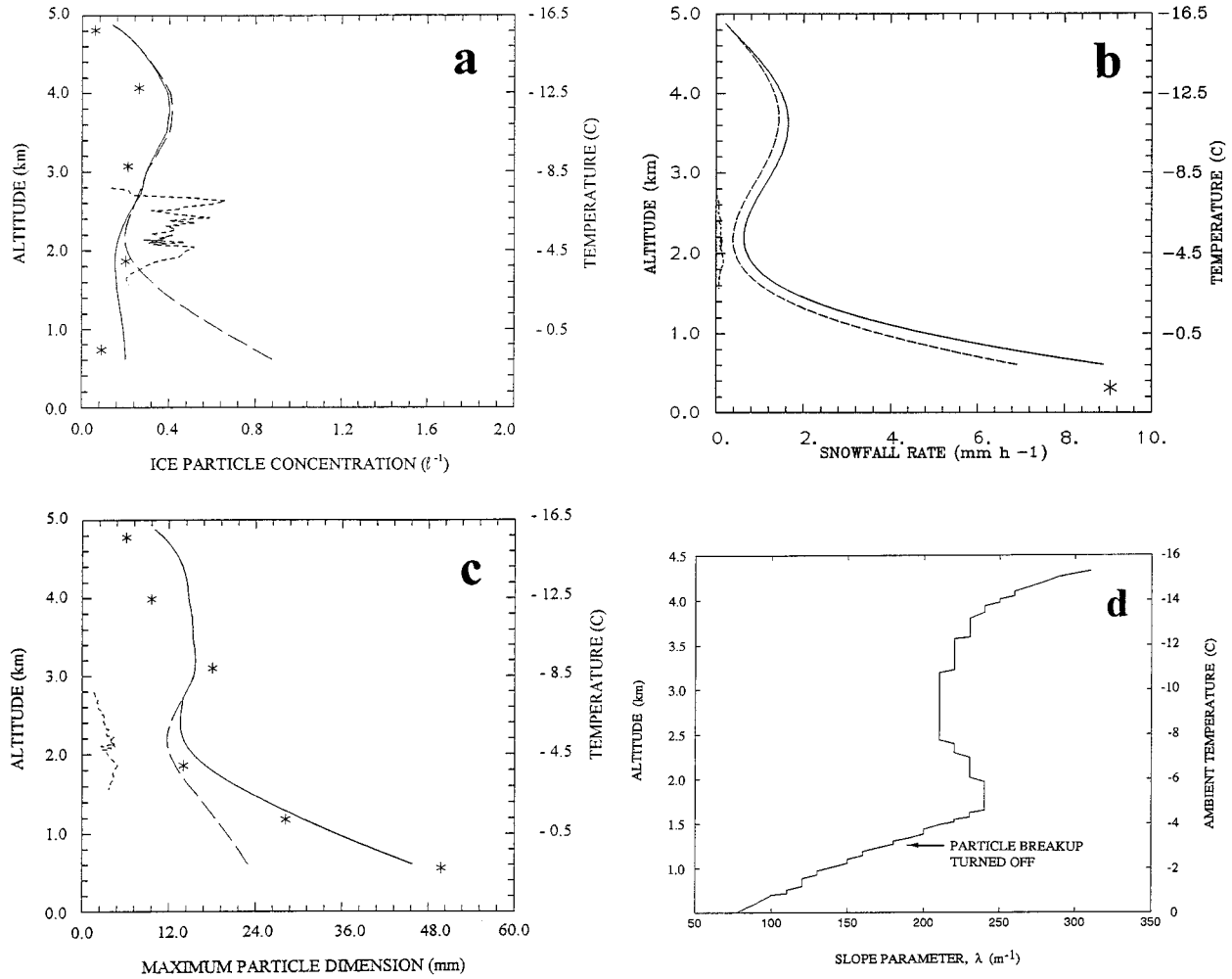

FIG. 16. Comparison of vertical profiles of (a) ice particle concentration derived from aircraft measurements (*), Mitchell model results with aggregation (solid line) and without aggregation (dashed line), and aircraft measurements from the WISP project (dashed line between 1.6 and 2.8 km); (b) snowfall rate in the same format as (a) except that the dashed line is for diffusional growth only and solid line is with accretion, and the * is a ground-based measurement of snowfall rate at St. John's airport; and (c) maximum particle dimension in the same format as (a). Mitchell model prediction of vertical profile of slope parameter (λ) applicable to Eq. (3) is shown in (d).

surface low, frontal boundaries, wind, and temperature fields.

2) A 5 km $\times$ 200 km vertical cross section through the model domain reproduced the general trend of sloping contours of temperature and equivalent potential temperature observed by dropsondes released from the aircraft.
3) The vertical velocity field generated by the model in the vicinity of the very large snowflakes agreed well with (limited) Doppler radar observations.

A synthesis of observations and model results has provided an explanation of the physics associated with the development of very large snowflakes in this CASP II winter storm. Figure 17 provides a simple schematic diagram of the origin and development of the very large snowflakes, and a chronology of the contributing processes is presented in the following summary.

A 990-mb low was centered about 300 km south of the southern coast of Newfoundland at 0000 UTC on 15 February 1992. Approximately 70 km west of the center of the low, a region of low-level convergence with light winds produced weak convective instability aloft from about 850 $\rightarrow$ 550 mb. Dendritic crystals grew to 3–5 mm within the region of weak convective instability in a water saturated environment with LWC $\sim$ 0.2 g m^{-3}. The dendrites were carried aloft and entrained into the 500-mb wind flow that was from the southwest at about 20–25 m s^{-1}. After being transported approximately 200 km downwind, the dendrites fell into a region containing needles and dendrites supported by an upward vertical velocity produced by low-level convergence. The temperature field along the direction of travel had downward sloping isotherms in the temperature range from about $-5 \rightarrow +2$°C. The slope of the

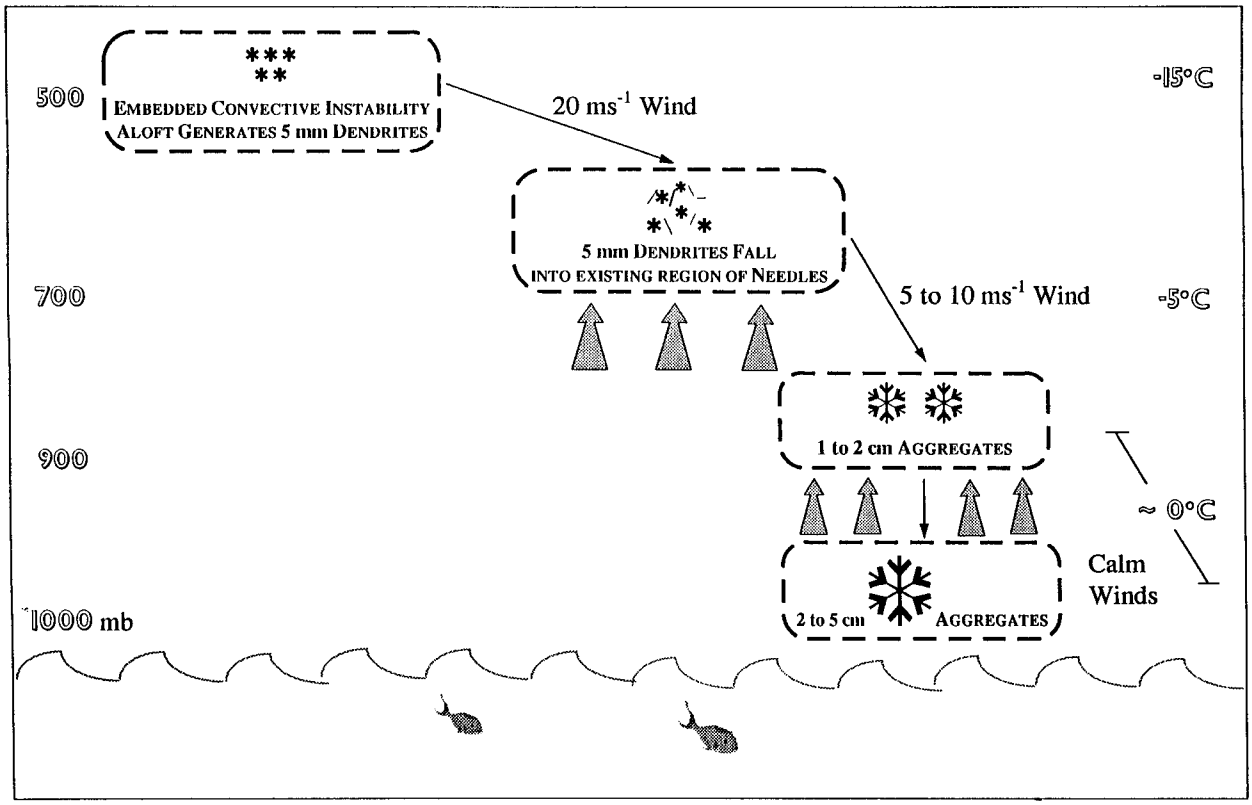

FIG. 17. Schematic drawing showing the evolution of 2–5 cm snowflakes. The broad vertical arrows represent vertical motion on the order of 0.5 m s^{-3} that retarded the fall velocity of the particles and supported an accumulation zone where rapid aggregation took place.

isotherms and the $\sim$0.5 m s^{-1} upward motion produced conditions within which the snowflakes slowly settled downward through the ambient field of ice and snow particles in a temperature regime conducive to rapid aggregation that had been developed in part through melting-layer diabatic processes. Theoretical and observational evidence suggests that particle breakup was essentially absent in this latter temperature regime and the aggregates eventually grew to 4–5 cm in the region between $-3°$ and $+2°$C. This scenario, based upon a very comprehensive approach, is consistent with the overall suggestions made by Stewart et al. (1990) who had examined another situation with very large snowflakes, although this earlier study was not able to quantify the processes to the degree achieved here.

It may well be that the combination of geographic features near the southern coast of the Canadian Maritimes and Newfoundland favors the development of very large snowflakes. The Gulf Stream maintains air temperatures to the south of this region at or slightly above 0°C during winter storms and this warm ocean also provides a ready, huge supply of moisture. This combination of temperature and moisture is conducive to the maintenance of a storm environment that is at or near saturation. Convective instability at upper levels that arises through the overall storm structure can lead to the generation of large numbers of millimeter-size dendritic ice particles. In the saturated atmosphere below their generation level, the copious quantities of ice particles melt and deepen the layer near 0°C, which in turn can act to modify the associated wind fields in the vicinity of the warm front (e.g., Szeto 1988a, b), so that the particles encounter gently ascending air near the melting layer. This chain of events leads to an environment favorable for rapid aggregation that produces very large snowflakes (and high precipitation rates) that rapidly accumulate at the surface.

Acknowledgments. The authors are grateful to Dr. George Isaac, Dr. Stewart Cober, Walter Strapp, and Bob Crawford of the Atmospheric Environment Service of Canada for their support in the field project and collaborating in the data analysis. We are indebted to Dr. J. A. Weinman of NASA Goddard Space Flight Center and Dr. J. L. Schols of General Sciences Corporation for supplying the analyzed SSM/I data, and to Dr. Dave Hudak of the University of Toronto for supplying the Doppler radar data. We also wish to thank Dr. David Mitchell and Dr. David Rogers for helpful discussions concerning data analysis. We are grateful to Dr. Roy Rasmussen of NCAR for reviewing the manuscript and providing helpful suggestions. This work was supported in part by the Federal Panel on Energy Research and Development (PERD) of Canada and by Grant No. ISI-

8922336 to SPEC Incorporated from the National Science Foundation.

REFERENCES

Abbe, C. A., Jr., 1915: Gigantic snowflakes. *Mon. Wea. Rev.,* **43,** 73.

Anthes, R. A., 1990: Recent applications of the Penn State/NCAR mesoscale model to synoptic, mesoscale and climate studies. *Bull. Amer. Meteor. Soc.,* **71,** 1610–1629.

——, and T. T. Warner, 1978: Development of hydrodynamic models suitable for air pollution and other mesometeorological studies. *Mon. Wea. Rev.,* **106,** 1045–1078.

Auer, A. H., Jr., 1971: Some large snowflakes. *Weather,* **26,** 121–122.

Baumgardner, D., and A. Rodi, 1989: Laboratory and wind tunnel evaluation of the Rosemount Icing Detector. *J. Atmos. Oceanic Technol.,* **6,** 971–979.

Cober, S. G., G. A. Isaac, and J. W. Strapp, 1995: Aircraft icing measurements in East Coast winter storms. *J. Appl. Meteor.,* **34,** 88–100.

Cooper, W. A., and R. P. Lawson, 1984: Physical interpretation of results from the HIPLEX-1 Experiment. *J. Appl. Meteor.,* **23,** 523–540.

Corliss, W. R., 1984: *Tornadoes, Dark Days, Anomalous Precipitation, and Related Weather Phenomena.* Sourcebook Project, 196 pp.

Denning, W. F., 1912: Large snowflakes. *Symon's Meteor. Mag.,* **47,** 22.

Diamond, M., and W. P. Lowry, 1954: Correlation of density of new snow with 700-millibar temperature. *J. Meteor.,* **11,** 512–513.

Dobrowolski, A. B., 1903: *La Neige et le Givre.* Vol. 3, *Rapports Scientifiques, Resultats du Voyagede S. Y. Belgica, 1897–1899,* J. E. Buschman, 78 pp.

Dudhia, J., 1993: A nonhydrostatic version of the Penn State/NCAR mesoscale model: Validation tests and simulation of an Atlantic cyclone and cold front. *Mon. Wea. Rev.,* **121,** 1493–1513.

Furukawa, Y., M. Yamamoto, and T. Kuroda, 1987: Ellipsometric study of the transition layer on the surface of an ice crystal. *J. Cryst. Growth,* **82,** 665–677.

Grell, G. A., 1993: Prognostic evaluation of assumptions used by cumulus parameterizations. *Mon. Wea. Rev.,* **121,** 764–787.

——, J. Dudhia, and D. R. Stauffer, 1994: A description of the fifth-generation Penn State/NCAR Mesoscale Model (MM5). NCAR Mesoscale and Microscale Meteorology Division Tech. Note NCAR/TM398+STR, 138 pp.

Gunn, K. L. S., and J. S. Marshall, 1958: The distribution with size of aggregate snowflakes. *J. Meteor.,* **15,** 452–461.

Hawke, E. L., 1951: Outsize snowflakes. *Weather,* **6,** 254.

Herzegh, P. H., and P. V. Hobbs, 1980: The mesoscale and microscale structure and organization of clouds and precipitation in midlatitude cyclones. II: Warm-frontal clouds. *J. Atmos. Sci.,* **37,** 597–611.

Heymsfield, A. J., 1986: Ice particle evolution in the anvil of a severe thunderstorm during CCOPE. *J. Atmos. Sci.,* **43,** 2463–2478.

——, and L. M. Miloshevich, 1989: Evaluation of liquid water measuring instruments in cold clouds sampled during FIRE. *J. Atmos. Oceanic Technol.,* **6,** 378–388.

Hobbs, P. V., and J. D. Locatelli, 1978: Rainbands, precipitation cores and generating cells in a cyclonic storm. *J. Atmos. Sci.,* **35,** 230–241.

——, and Coauthors, 1971: Contributions from the Cloud Physics Group. Res. Rep. VI: Studies of winter cyclonic storms over the Cascade Mountains, 1970–1971. 305 pp. [Available from Tech. Rep., Department of Atmospheric Sciences, University of Washington, Seattle, WA, 98195.]

——, H. Harrison, and E. Robinson, 1974: Atmospheric effects of pollutants. *Science,* **183,** 909–915.

Holroyd, E. W., III, 1971: The meso- and micro-scale structure of Great Lakes snowstorm bands—a synthesis of ground measurements, radar data, and satellite observations. Ph.D. dissertation, College of Arts and Sciences, State University of New York at Albany, 148 pp.

Isaac, G. A., 1991: Microphysical characteristics of Canadian Atlantic storms. *Atmos. Res.,* **26,** 339–360.

Jiusto, J. E., 1971: Crystal development and glaciation of a supercooled cloud. *J. Rech. Atmos.,* **5,** 69–85.

King, W. D., D. A. Parkin, and R. J. Handsworth, 1978: A hot wire liquid water device having fully calculable response characteristics. *J. Appl. Meteor.,* **17,** 1809–1813.

Knollenberg, R. G., 1970: The optical array: An alternative to scattering or extinction for airborne particle size determination. *J. Appl. Meteor.,* **9,** 86–103.

——, 1981: Techniques for probing cloud microstructure. *Clouds, Their Formation Optical Properties and Effects,* P. V. Hobbs and A. Deepak, Eds., Academic Press, 15–92.

Lawson, R. P., R. E. Stewart, J. W. Strapp, and G. A. Isaac, 1993a: Airborne measurements of the origin and growth of very large snowflakes. *Geophys. Res. Lett.,* **20,** 53–56.

——, R. H. Cormack, and K. A. Weaver, 1993b: A new airborne precipitation spectrometer for atmospheric research. Preprints, *Eighth Symp. Meteorological Observations and Instrumentation,* Anaheim, CA, Amer. Meteor. Soc., 30–35.

Lo, K. K., 1983: Growth processes of snow. Ph.D. thesis, Massachusetts Institute of Technology, 192 pp.

——, and R. E. Passarelli, Jr., 1981: Height evolution of snow-size distributions. Preprints, *20th Conf. on Radar Meteorology,* Boston, MA, Amer. Meteor. Soc., 397–401.

——, and ——, 1982: The growth of snow in winter storms: An airborne observational study. *J. Atmos. Sci.,* **39,** 697–706.

Lowe, E. J., 1887: Snowstorm of January 7, 1887. *Nature,* **35,** 271.

Magono, C., 1953: On the growth of snowflake and graupel. *Sci. Rep., Yokohama Natl. Univ.,* **1,** 18–40.

——, 1960: Structure of snowfall revealed by geographic distribution of snow crystals. *Physics of Precipitation, Geophys. Monogr.,* No. 5, Amer. Geophys. Union, 142–161.

——, and T. Nakamura, 1965: Aerodynamic studies of falling snowflakes. *J. Meteor. Soc. Japan,* **43,** 139–147.

——, and C. W. Lee, 1966: Meteorological classification of natural snow crystals. *J. Fac. Sci., Hokkaido Imp. Univer.,* Ser. VII, **2,** 321–362.

Mitchell, D. L., 1988: Evolution of snow-size spectra in cyclonic storms. Part I: Snow growth by vapor deposition and aggregation. *J. Atmos. Sci.,* **45,** 3431–3451.

——, 1990: Evolution of snow-size spectra predicted by the growth processes of diffusion, aggregation and riming. Preprints, *Conf. on Cloud Physics,* San Francisco, CA, Amer. Meteor. Soc., 270–277.

——, 1991: Evolution of snow-size spectra in cyclonic storms. Part II: Deviations from the exponential form. *J. Atmos. Sci.,* **48,** 1885–1899.

——, 1994: A model predicting the evolution of ice particle size spectra and radiative properties of cirrus clouds. Part I: Microphysics. *J. Atmos. Sci.,* **51,** 797–816.

——, 1995: An analytical model predicting the evolution of ice particle size distributions. Ph.D. dissertation, University of Nevada at Reno, 171 pp.

Pike, W. S., 1988: Unusually-large snowflakes. *J. Meteor.,* **13,** 3–16.

Plunket, J. D., 1891: Snowfalls. *Mon. Wea. Rev.,* **19,** 11.

Power, B. A., 1962: Relationship between density of newly fallen snow and form of snow crystals. *Nature,* **193,** 1171.

Pruppacher, H. R., and J. D. Klett, 1978: *Microphysics of Clouds and Precipitation.* D. Reidel, 707 pp.

Rauber, R. M., 1987: Characterization of cloud ice and precipitation during wintertime over the mountains of northern Colorado. *J. Appl. Meteorol.,* **26,** 488–524.

——, 1985: Physical structure of northern Colorado river basin cloud systems. Ph.D. dissertation, Colorado State University, Ft. Collins, CO, 362 pp.

Rogers, D. C., 1973: The aggregation of natural ice crystals. M.S.

thesis, Dept. of Atmospheric Resources, University of Wyoming, 91 pp.

Schols, J. L., J. A. Weinman, G. D. Alexander, R. E. Stewart, L. J. Angus, and A. C. L. Lee, 1998: Microwave properties of frozen precipitation around a North Atlantic cyclone. *J. Appl. Meteorol.*, in press.

Stewart, R. E., 1984: Deep 0°C isothermal layers within precipitation bands over southern Ontario. *J. Geophys. Res.*, **89,** 2567–2572.

——, 1991: Canadian Atlantic Storms Program: Progress and plans of the meteorological component. *Bull. Amer. Meteor. Soc.,* **72,** 364–371.

——, 1992: Precipitation types in the transition region of winter storms. *Bull. Amer. Meteor. Soc.,* **73,** 287–296.

——, and R. W. Crawford, 1995: Some characteristics of the precipitation formed within winter storms over eastern Newfoundland. *Atmos. Res.*, **36,** 17–37.

——, J. D. Marwitz, J. C. Pace, and R. E. Carbone, 1984: Characteristics through the melting layers of stratiform clouds. *J. Atmos. Sci.,* **41,** 3227–3237.

——, R. W. Shaw, and G. A. Isaac, 1987: Canadian Atlantic Storms Program: The Meteorological Field Project. *Bull. Amer. Meteor. Soc.,* **68,** 338–345.

——, R. W. Crawford, and N. R. Donaldson, 1990: Precipitation characteristics within several Canadian East Coast winter storms. *Atmos. Res.,* **25,** 293–316.

Szeto, K. K., and R. E. Stewart, 1997: Effects of melting on frontogenesis. *J. Atmos. Sci.,* **54,** 689–702.

——, C. A. Lin, and R. E. Stewart, 1988a: Mesoscale circulations forced by melting snow. Part I. Basic simulations and dynamics. *J. Atmos. Sci.,* **45,** 1629–1641.

——, R. E. Stewart, and C. A. Lin, 1988b: Mesoscale circulations forced by melting snow. Part II. Application to meteorological features. *J. Atmos. Sci.,* **45,** 1642–1650.

Thomson, A. D., and R. List, 1996: Raindrop spectra and updraft determination by combining Doppler radar and distrometer. *J. Atmos. Oceanic Technol.,* **13,** 465–476.